ANL-6795

IRRADIATION BEHAVIOR OF URANIUM-FISSIUM ALLOYS

J. H. Kittel, J. A. Horak,
W. N. Beck, and R. J. Fousek

ARGONNE NATIONAL LABORATORY, ARGONNE, ILLINOIS

Printed in the United States of America
Available from
National Technical Information Service
U.S. Department of Commerce
5285 Port Royal Road
Springfield, Virginia 22151
Price: Printed Copy $3.00; Microfiche $0.95

ANL-6795
Reactor Technology

ARGONNE NATIONAL LABORATORY
9700 South Cass Avenue
Argonne, Illinois 60439

IRRADIATION BEHAVIOR OF URANIUM-FISSIUM ALLOYS

by

J. H. Kittel,* J. A. Horak,**
W. N. Beck,* and R. J. Fousek†

EBR-II Project

October 1971

*Formerly Materials Science Division
**Formerly Materials Science Division. Now with Dept. of Nuclear Engineering, University of New Mexico.
†Materials Science Division

2

TABLE OF CONTENTS

LIST OF FIGURES

LIST OF FIGURES

LIST OF FIGURES

LIST OF TABLES

IRRADIATION BEHAVIOR OF URANIUM-FISSIUM ALLOYS

by

J. H. Kittel, J. A. Horak,
W. N. Beck, and R. J. Fousek

ABSTRACT

A series of uranium-fissium and uranium-fissium-zirconium alloys was irradiated in thermal test reactors to study the relationship of dimensional stability to alloy composition, thermal cycling, burnup, irradiation temperature, postirradiation heating, and cladding restraint. Uranium-atom burnups as high as 6.2% were achieved, and center fuel temperatures were in the range of 170-790°C. None of the alloy compositions tested showed irradiation behavior superior to the uranium-5 wt % fissium alloy that has been used as driver fuel in EBR-II since it began operation. This alloy is among those uranium-base alloys most capable of resisting high-temperature irradiation swelling. None of the alloys showed evidence of the reversion to the metastable gamma phase that has been observed in comparable uranium-molybdenum alloys. Swelling of uranium-fissium alloys was effectively restrained by most of the 0.009-in.-thick cladding materials investigated. Local hydrostatic forces due to swelling of the fuel caused the fuel to extrude extensively out of small vent holes in the cladding. Little axial fuel movement occurred within the cladding, however, even when the upper fuel surface was entirely unrestrained.

I. INTRODUCTION

EBR-II (Experimental Breeder Reactor No. II) was originally designed and constructed by Argonne National Laboratory to provide a small-plant demonstration of a sodium-cooled fast-breeder-reactor power plant with a "quick-turnaround" fuel cycle. The thermal power output of the reactor is 62.5 MW. Following successful demonstration of the plant and the fuel cycle, the plant was adapted to serve as a fast-reactor irradiation test facility.

The metallic uranium-fissium alloy originally specified to fuel EBR-II to demonstrate the "quick turnaround" has been retained as the

driver fuel for operation of EBR-II as a test reactor. The relatively low cost of the fuel, its demonstrated reliability, and its desirable neutronic characteristics made it the preferred choice for continued operation of the reactor.

Uranium-fissium alloy is a product of the on-site pyrometallurgical reprocessing facility. Until recently, discharged fuel from the reactor was remotely processed, fabricated, and assembled into fuel elements in this facility for reinsertion into the reactor.

During pyrometallurgical reprocessing of the uranium, most of the fission products are removed from the molten fuel in a zirconia crucible by a melt-refining process. Relatively volatile fission products such as cesium and the rare gases boil off. Barium, strontium, and the rare-earth metals form adherent reaction layers with the wall of the zirconia crucible. The fission products remaining in the melt are principally zirconium, niobium, molybdenum, technetium, ruthenium, rhodium, and palladium. These elements cannot be removed from uranium by oxidative slagging, because the free energies of formation of their oxides are too close to that of uranium oxide. Zirconium, however, can be removed if desired by a drossing reaction with carbon.

This group of fission products that remain in the fuel have been termed "fissium" (symbol Fs). During repeated fuel recycling, the concentration of fissium in the alloy will build up to an equilibrium level that depends upon the frequency of reprocessing and the amount of fresh fuel added during each reprocessing cycle. The ratios of fission products comprising the fissium, however, will remain relatively constant. Their relative proportions, in weight percent, are approximately 1.3 zirconium, 0.1 niobium, 43.2 molybdenum, 12.5 technetium, 33.2 ruthenium, 5.9 rhodium, and 3.8 palladium.

The fissium elements were to be allowed to accumulate at a level of ~5 wt % in the EBR-II uranium driver fuel. A synthetic U-5 wt % Fs alloy was specified for the original driver fuel[1] to minimize changes in fuel properties with repeated recycling of the fuel. Natural isotopes of the fissium elements were used in the synthetic fuel, and additional amounts of molybdenum and ruthenium were used as a substitute for technetium. Experimental studies have shown that the properties of uranium-fissium alloys in which molybdenum and ruthenium are substituted for technetium do not differ significantly from those of uranium-fissium alloys containing normal amounts of technetium.[2] Synthetic fissium alloys were also used for the study reported here. A typical fissium composition in the synthetic alloys is, in weight percent, 49.2 molybdenum, 3.6 palladium, 6.0 rhodium, 40.2 ruthenium, and 1.0 zirconium.

The operating cost of EBR-II can be lowered by increasing the achievable burnup in the uranium-fissium alloy driver fuel (now being procured from commercial sources). Interest has therefore continued in the results of an extensive series of irradiation experiments that examined the effects of high burnup on several different uranium-fissium alloys. Most of the results of these experiments have been previously reported only in internal memoranda. This report has been compiled to collect the results into a single document and to make the information more readily available. Results have previously been published on more limited irradiation studies on uranium-fissium alloys[3-5] as well an on uranium-plutonium-fissium alloys.[5-9]

The experiments described in this report were concerned primarily with the dimensional stability of uranium-fissium alloys as affected by irradiation conditions, alloy composition, and cladding restraint.

II. PROPERTIES OF URANIUM-FISSIUM ALLOYS

The physical properties, transformation kinetics, and microstructures of uranium-fissium alloys have been reported in detail.[10-13] Phase relations in the uranium-fissium system have been shown to parallel closely those in the U-Mo-Ru ternary system. The developed microstructure is quite sensitive to cooling rate. Upon rapid cooling, the high-temperature gamma phase is retained as a metastable solid solution at room temperature. This phase is characterized by low hardness and low density. Slower cooling rates result in precipitation of U_2Ru from the gamma solid solution and partial transformation of gamma to alpha uranium at lower temperatures. The latter is a harder, higher-density phase.

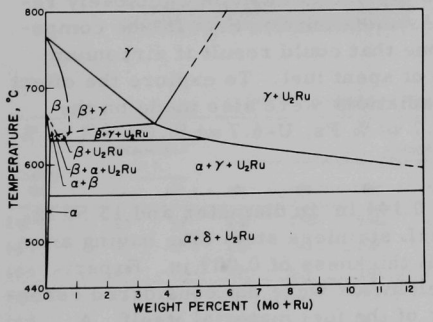

Fig. 1. Vertical Section through the Uranium-rich Corner of the U-Mo-Ru Ternary System at a Mo/Ru Weight Ratio of 1.25 (from Ref. 13). Neg. No. MSD-30162.

The uranium-rich corner of the U-Mo-Ru ternary system is shown in Fig. 1.[14] The portion of the vertical section shown is that in which the weight ratio of molybdenum to ruthenium is 1.25, which approximates that in the fissium alloys.

Although pure gamma uranium is unstable below 769°C, the alloyed gamma phase in uranium-fissium alloys persists as a stable phase down to 552°C. The temperature at which beta phase forms is lowered from 759 to 682°C by only 3 wt % fissium. Formation of the beta phase is entirely suppressed by higher

fissium contents, the gamma phase, on cooling, transforms directly to alpha. Other phases found in uranium-fissium alloys are U_2Ru, ZrRu, and a low-temperature phase that is isostructural with the delta phase in the uranium-molybdenum system.

On cooling U-5 wt % Fs alloy (the alloy of greatest interest), single-phase gamma is stable down to 725°C. With slow cooling, precipitation of U_2Ru begins at 725°C and continues down to 642°C, at which temperature gamma begins to reject alpha. The formation of delta begins at 552°C. With normal cooling rates associated with injection casting, however, U-5 wt % Fs alloy does not completely transform and is, in fact, predominantly gamma.

If zirconium were not removed during reprocessing, the composition of the fuel could be designated as a uranium-fissium-zirconium alloy. Under these circumstances, the additional zirconium could be present in amounts as great as half the total fissium content, so the equilibrium fuel composition could be U-5 wt % Fs-2.5 wt % Zr. In contrast to the uranium-fissium alloys, alloys of the uranium-fissium-zirconium type are predominantly alpha phase because the zirconium removes ruthenium, a gamma-phase stabilizing element, from the gamma solid solution to form the compound ZrRu.

III. SPECIMEN MATERIALS

Most of the experimental irradiations in the present study were made on the EBR-II driver fuel alloy, U-5 wt % Fs, and on the closely related alloy U-5 wt % Fs-2.5 wt % Zr. As mentioned in Sec. II, the composition of the latter alloy is similar to one that could result if zirconium were not removed during reprocessing of spent fuel. To explore the effect of wider variations in composition, irradiations were also made on the alloys U-3.3 wt % Fs-1.7 wt % Zr, U-3.7 wt % Fs, U-6.7 wt % Fs-3.3 wt % Zr, and U-10 wt % Fs-5 wt % Zr.

The EBR-II Mark IA fuel pin is 0.144 in. in diameter and 13.50 in. long. It is sodium-bonded to a Type 304L stainless steel tube having an internal diameter of 0.156 in. and a wall thickness of 0.009 in. Experimental irradiations of full-length fuel elements were not considered essential to evaluate the irradiation behavior of the fuel material itself. A shorter length, 1.00 in., was therefore selected as a convenient specimen size that could be adapted in multiple numbers for capsule irradiations.

It was considered essential, however, that the diameter of the specimens matched that of an actual reactor fuel pin and that the specimens were made by the fabrication procedure used for the actual pin. This requirement was met by producing a number of full-length fuel pins and cutting them into the shorter length for irradiation. The injection-casting process,[15]

which had been selected for remotely fabricating the fuel pins for EBR-II, was used to produce the full-length pins. In this process, Vycor glass molds, approximately 17 in. long, are suspended, open ends down, above the crucible. The fuel alloy is melted and heated to the desired casting temperature under a protective atmosphere. The furnace is then evacuated, and the crucible is raised to submerge the open mold tips in the melt. After a predetermined delay of a few seconds, the furnace is then pressurized to force molten-metal columns upward in the evacuated molds. After the charge has been cooled to room temperature and removed from the furnace, the molds are broken away from the castings. The castings are about 16 in. long.

Master alloys of the highest alloy contents were made first and analyzed. Succeeding alloys were then made by dilution. The master alloys were vacuum-melted in magnesia crucibles and bottom-poured into thoria-coated graphite molds. For injection casting, the master alloys were melted with uranium dilutions as required in thoria-coated graphite under vacuums near 8×10^{-4} mm Hg. Casting temperatures were near 1350°C, so most of the compositions had 300°C of superheat. Two ^{235}U enrichments, 10 and 20%, were used. Table I shows the analyzed compositions of the castings used in the investigation. Subsequent tables of experimental results in this report show the casting number as part of the original specimen number. The location and top-and-bottom orientation of each specimen in the original injection casting were noted.

Figure 2 shows a typical specimen before irradiation.

Fig. 2

Typical Specimen before Irradiation.
Mag. 2X. Neg. No. MSD-23438.

TABLE I. Composition of Alloys Used for Irradiation Specimens

Casting No.	Nominal Composition,[a] wt %		Composition,[a] wt %							Uranium Isotopic Composition,[b] at. %		
	Fs	Zr	Mo	Pd	Rh	Ru	Zr	C, ppm	N, ppm	^{234}U	^{235}U	^{236}U
E-3F-1C	3.3	1.7	1.64	0.124	0.148	1.28	1.58	24	c	0.887	10.24	0.047
1-E-2	3.7	0	1.67	0.18	0.23	1.68	0.03	c	c	0.113	10.4	0.0492
1-E-3	3.7	0	1.67	0.16	0.26	1.64	0.03	c	c	0.115	10.5	0.0494
1-E-4	3.7	0	c	c	c	c	c	c	c	c	c	c
1-E-5	3.7	0	c	c	c	c	c	c	c	c	c	c
E-16F-236	5	0	2.46	0.185	0.302	2.01	0.049	660	11	0.115	10.55	0.047
E-B16F-235	5	0	2.46	0.482	0.805	1.12	0.193	59	22	0.201	20.26	0.107
E-3F-1B	5	2.5	2.50	0.198	0.288	2.06	2.60	18	22	0.103	10.70	0.051
E-3F-1A	5	2.5	2.46	0.194	0.281	2.01	2.61	14	20	0.203	20.42	0.106
E-SF-2A	6.7	3.3	3.30	0.263	0.363	2.74	3.50	22	26	0.100	10.24	0.050
E-SF-1A	10	5	5.13	0.412	0.562	4.24	5.39	31	11	0.098	10.02	0.048

[a]Balance uranium.
[b]Balance ^{238}U.
[c]Not available.

IV. IRRADIATION PROCEDURE

Before irradiation, each specimen was measured for dimensions, weight, density, and hardness. The densities were determined by weight loss while the specimens were immersed in CCL_4. All specimens were radiographed for detection of internal porosity. Metallographic examinations were made on representative castings of each melt. No machining was done on the outer diameter of the fuel specimens, nor was any further heat treatment performed.

All specimens were irradiated in capsules while they were submerged in NaK. Most of the irradiations were made in uninstrumented capsules in the MTR (Materials Testing Reactor). Figure 3 shows the design of a typical MTR capsule. Preliminary values of burnup were obtained from values of thermal-neutron flux indicated by flux monitors made of cobalt-0.1 wt % aluminum alloy. Final values of burnup were obtained from determination of the changes in uranium isotope ratios, using the relation[16]

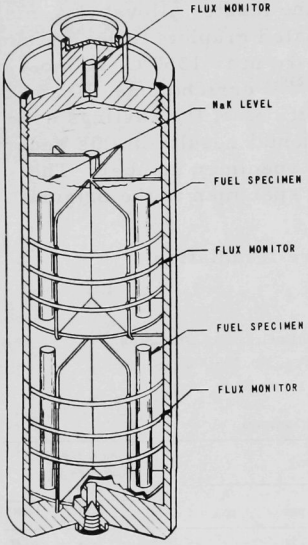

Fig. 3. Irradiation Capsule Used for MTR Irradiations. ANL Neg. No. 106-4083.

$$F_5 = N_8^0[(R_{5/8}^0 - R_{5/8}) - (R_{6/8} - R_{6/8}^0)],$$

where

F_5 = at. % fission due to ^{235}U,

N_8^0 = at. % ^{238}U in preirradiated fuel,

$R_{5/8}^0$ = initial $^{235}U/^{238}U$ atom ratio,

$R_{5/8}$ = final $^{235}U/^{238}U$ atom ratio,

$R_{6/8}^0$ = initial $^{236}U/^{238}U$ atom ratio,

and

$R_{6/8}$ = final $^{236}U/^{238}U$ atom ratio.

From the analyzed atom burnup of the uranium, it was possible to calculate the perturbed flux and hence the maximum power density for the fuel specimens. The dependence of surface and center temperatures of the specimen on power density was experimentally determined in a series of instrumented capsules in the CP-5 reactor. Small-diameter thermocouples were located in the centers of fuel specimens and in the NaK adjacent to the specimens.

Near the latter part of this investigation, the CP-5 reactor fuel elements were modified[17] so that instrumented temperature-controlled capsules[18] could be accommodated. The final experimental irradiations of

uranium-fissium alloys were performed in these facilities, including all experiments in which the fuel specimens were clad. Figure 4 shows a typical CP-5 capsule assembly. As for the MTR capsules, the relationship between the surface and center temperatures of the specimen and the power density was determined by thermocouples in the centers of the specimens and in the NaK adjacent to the specimens.

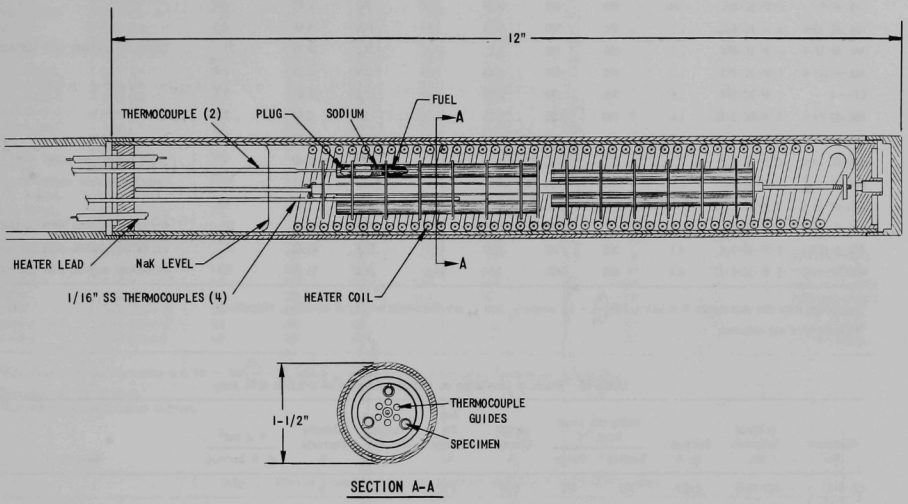

Fig. 4. Irradiation Capsule Used for CP-5 Irradiations. ANL Neg. No. 106-6079 Rev. 1.

The MTR irradiations were made on specimens enriched to 10% ^{235}U. The CP-5 irradiations were made on specimens with ^{235}U enrichments of both 10 and 20%. Use of the more highly enriched specimens enabled high fuel burnups to be achieved with irradiation times of 12-14 months.

The same measurements as those made before irradiation (with the exception of hardness) were made on all irradiated specimens. After irradiation, all capsules were opened and the contents examined under an inert atmosphere. Considerable use was made of a pinhole autoradiographic technique[19] for nondestructively determining the condition of the specimens before the capsules were opened. This technique was also used to determine nondestructively the length of the fuel column in the clad specimens after irradiation.

V. RESULTS AND DISCUSSION

A. Unclad Specimens

Tables II-VII summarize the irradiation conditions and the information obtained on each specimen. Figures 5-10 show photographs of typical

TABLE II. Effects of Irradiation on Unclad Specimens of U-3.3 wt % Fs-1.7 wt % Zr Alloy

Specimen No.	Original Specimen No.	Burnup, at. %	Midlength Irrad Temp, °C		Length Change, %	Avg Dia Change, %	Weight Change, mg	Density Decrease, %	% Δ Vol[a] at. % Burnup	Remarks
			Surface	Center						
CP-3-1	E-3F-1C-5-2	0.025	395	420	0.36	0.91	-0.6	b	-	
CP-5-2	E-3F-1C-5-3	0.27	570	610	0.13	1.18	-0.7	0.78	2.8	
CP-2-5	E-3F-1C-5-1	0.45	285	305	2.99	-0.42	0.7	1.94	4.4	
ANL-42-22-6	E-3F-1C-1-12	0.85	240	260	0.99	5.76	-2.1	4.59	5.7	
ANL-42-9-5	E-3F-1C-8-1	0.86	380	420	0.89	1.12	-0.2	2.91	3.5	
ANL-42-10-6	E-3F-1C-8-2	1.1	470	520	0.78	1.81	-1.1	4.57	4.3	
ANL-42-12-4	E-3F-1C-8-4	1.1	650	700	4.7	12.8	-224.1	18.95	21	Uniformly swelled, with surface cracks.
ANL-6-117-4	E-3F-1C-1-3	1.2	370	410	1.44	2.23	-0.9	2.85	2.4	
CP-7-4	E-3F-1C-5-4	1.6	355	390	2.75	4.45	25.2	12.81	9.3	
ANL-42-24-4	E-3F-1C-1-11	1.6	390	420	0.88	0.76	-1.4	3.91	2.6	
ANL-6-115-4	E-3F-1C-1-2	2.0	500	560	5.34	3.34	-0.7	17.23	9.6	
ANL-42-14-6	E-3F-1C-8-6	2.3	380	410	4.99	5.45	-0.8	16.40	9.9	Small bulge near upper end.
ANL-42-16-4	E-3F-1C-8-8	2.6	430	480	10.12	11.9	12.5	60.58	58	Large bulge near upper end.
ANL-42-18-6	E-3F-1C-8-10	3.1	340	380	0.24	3.35	-5.0	15.28	5.8	
ANL-6-113-4	E-3F-1C-1-1	3.8	480	530	0.99	21.9	-27.1	31.47	12	Uniformly swelled, with surface cracks.
ANL-6-123-1	E-3F-1C-1-6	4.1	500	540	7.81	13.5	57.6	43.22	17	Uniformly swelled, with surface cracks.
ANL-42-19-3	E-3F-1C-8-11	4.9	600	650	7.54	19.6	8.6	33.10	9.3	Uniformly swelled, with surface cracks.

[a]Calculated from the expression $\% \Delta \text{ Vol} = 100\left(\frac{\rho_i}{\rho_f} - 1\right)$, where ρ_i and ρ_f are the initial and final densities, respectively.

[b]Measurement not obtained.

TABLE III. Effects of Irradiation on Unclad Specimens of U-3.7 wt % Fs Alloy

Specimen No.	Original Specimen No.	Burnup, at. %	Midlength Irrad Temp, °C		Length Change, %	Avg Dia Change, %	Weight Change, mg	Density Decrease, %	% Δ Vol[a] at. % Burnup	Remarks
			Surface	Center						
CP-3-4	1E2-11-5	0.025	395	420	0.10	1.52	-1.6	b	-	
CP-2-1	1E2-11-4	0.43	310	355	0.39	0.49	-8.7	1.36	3.2	
ANL-42-11-6	1E2-12-3	0.65	400	430	5.28	12.0	-458.0	b	-	
ANL-6-119-5	1E2-2-4	0.67	230	240	0.08	1.04	0.3	0.82	1.2	
ANL-42-9-4	1E2-12-1	0.85	390	420	-0.26	0.69	-0.2	1.80	2.2	
ANL-42-10-5	1E2-12-2	1.1	480	520	0.38	0.21	-1.7	3.21	3.0	
ANL-42-12-3	1E2-12-4	1.2	690	740	9.01	14.8	72.3	27.05	31	Uniformly swelled, with surface cracks.
ANL-42-15-6	1E2-12-7	1.4	270	290	2.80	11.4	0.5	16.94	15	
CP-7-1	1E2-11-7	1.6	380	420	5.25	10.1	17.4	19.91	16	
ANL-42-23-6	1E2-11-2	1.6	410	450	0.82	3.33	0.9	8.46	5.6	
ANL-42-22-5	1E2-11-1	1.7	450	490	0.61	2.01	-1.3	4.60	2.7	
ANL-6-122-5	1E2-2-10	2.0	520	560	11.7	11.9	150.3	48.37	47	Swelled near upper end.
ANL-42-14-5	1E2-12-6	2.3	400	430	2.58	6.45	-1.2	17.63	11	
ANL-42-17-4	1E2-12-9	3.0	500	540	12.7	36.2	139.8	25.55	12	Swelled near upper end.
ANL-42-18-5	1E2-12-10	3.1	350	380	0.73	3.6	-1.9	7.75	2.7	
ANL-6-113-1	1E2-2-1	3.4	430	460	1.66	18.8	6.4	20.05	7.4	
ANL-6-123-5	1E2-2-12	3.7	470	500	8.66	24.5	33.6	45.15	22	Swelled near upper end.
ANL-42-19-6	1E2-12-11	4.9	630	680	8.79	40.7	112.7	45.84	17	Swelled near center.

[a]Calculated from the expression $\% \Delta \text{ Vol} = 100\left(\frac{\rho_i}{\rho_f} - 1\right)$, where ρ_i and ρ_f are the initial and final densities, respectively.

[b]Measurement not obtained.

TABLE IV. Effects of Irradiation on Unclad Specimens of U-5 wt % Fs Alloy

Specimen No.	Original Specimen No.	Burnup, at. %	Midlength Irrad Temp, °C		Length Change, %	Avg Dia Change, %	Weight Change, mg	Density Decrease, %	% Δ Vol[a] at. % Burnup	Remarks
			Surface	Center						
CP-3-2	E-B16F-236-5-8	0.025	395	420	-0.06	0.14	-7.3	b	-	
CP-3-6	E-B16F-236-4-9	0.025	395	420	0.18	1.17	-4.1	b	-	
CP-4-5	E-B16F-236-4-10	0.19	560	600	0.02	0.76	-6.5	b	-	
CP-4-1	E-B16F-236-5-9	0.19	560	600	-0.14	0.90	-3.7	b	-	
CP-1-6	E-B16F-236-7-8	0.36	315	335	0.14	0.21	-2.4	0.98	2.7	
CP-1-2	E-B16F-236-7-2	0.36	260	275	2.06	2.56	-8.7	2.9	7.9	
CP-2-3	E-B16F-236-4-8	0.45	335	355	0.27	-0.42	-1.3	0.62	1.4	
ANL-6-119-2	E-B16F-236-13-1	0.64	200	220	1.73	0.21	-0.3	0.89	1.4	
CP-6-5	E-B16F-236-5-11	0.68	700	750	6.27	4.83	7.5	12.9	19	
CP-11-4	E-B16F-236-5-1	0.79	510	540	0.73	1.45	0.8	1.24	1.6	
CP-6-1	E-B16F-236-5-7	0.79	700	750	4.39	5.96	-1.1	13.9	18	
ANL-42-8-6	E-B16F-236-4-4	0.94	240	260	0.27	2.36	-1.7	1.58	1.7	
ANL-6-117-5	E-B16F-236-1-10	1.0	300	320	2.07	-0.35	-1.1	1.72	1.8	
ANL-6-116-5	E-B16F-236-1-8	1.2	340	370	2.81	-0.41	-0.8	2.4	1.9	
ANL-42-12-1	E-B16F-236-7-4	1.2	690	780	-15.7	7.43	-1017.1	29	23	
ANL-6-116-2	E-B16F-236-1-7	1.2	350	380	5.17	-0.90	-0.8	2.2	1.8	
ANL-42-9-1	E-B16F-236-7-1	1.5	630	680	1.66	6.97	-1.4	14.3	9.7	
CP-7-5	E-B16F-236-5-13	1.6	370	390	1.66	2.75	16.3	5.0	3.1	
CP-7-3	E-B16F-236-5-12	1.6	395	420	2.41	4.28	22.7	10.3	6.5	
ANL-42-6-6	E-B16F-236-4-2	2.0	480	510	1.96	2.35	3.5	7.6	3.7	
ANL-6-115-5	E-B16F-236-1-6	2.0	510	550	3.93	3.66	-1.9	10.0	4.9	
ANL-42-14-1	E-B16F-236-7-6	2.4	420	450	2.33	6.74	b	17[c]	7.0[c]	
ANL-6-113-2	E-B16F-236-1-1	3.4	430	460	6.13	7.08	-68.2	14.8	4.3	
ANL-42-7-6	E-B16F-236-4-3	3.7	480	510	2.97	1.44	-2.8	10.3	2.7	
ANL-42-5-6	E-B16F-236-4-1	4.5	550	590	6.60	4.75	-8.9	48	9.7	Severely warped.
CP-9-1	E-B16F-235-4-11	5.6	740	790	b	b	b	83	15	In three pieces.
CP-9-3	E-B16F-235-4-13	5.6	740	790	21.1	62.5	34	183	33	Uniformly swelled.
CP-9-5	E-B16F-235-4-8	5.8	720	760	11.5	50	74	136	25	Uniformly swelled.
CP-8-5	E-B16F-235-4-10	5.8	630	670	b	b	b	182	32	In four pieces.
CP-8-4	E-B16F-235-4-12	5.8	640	680	b	b	b	127	22	In three pieces.
CP-8-3	E-B16F-235-4-9	6.2	630	670	b	b	b	152	25	In three pieces.

[a]Calculated from the expression $\% \Delta \text{ Vol} = 100\left(\frac{\rho_i}{\rho_f} - 1\right)$, where ρ_i and ρ_f are the initial and final densities, respectively.

[b]Measurement not obtained.

[c]Calculated from dimensional changes.

TABLE V. Effect of Irradiation on Unclad Specimens of U-5 wt % Fs-2.5 wt % Zr Alloy

Specimen No.	Original Specimen No.	Burnup, at. %	Midlength Irrad Temp, °C		Length Change, %	Avg Dia Change, %	Weight Change, mg	Density Decrease, %	% Δ Vol[a] at. % Burnup	Remarks
			Surface	Center						
CP-3-5	E-3F-1B-8-9	0.025	395	420	0.25	-2.83	-1.1	b	-	
CP-3-2	E-3F-1B-13-7	0.025	395	420	0.26	1.89	-1.1	0.12	4.8	
CP-4-2	E-3F-1B-13-8	0.19	560	600	1.01	0.97	-0.7	2.28	12	
CP-5-3	E-3F-1B-13-10	0.26	570	610	0.61	0.76	-0.5	0.67	2.5	
CP-5-4	E-3F-1B-8-11	0.26	570	610	0.78	1.12	0.2	0.91	3.4	
CP-12-2	E-3F-1B-9-6	0.29	610	650	0.04	2.10	19.1	1.19	4.1	
CP-1-1	E-3F-1B-13-9	0.35	260	275	0.49	0.84	1.3	2.19	6.6	
CP-2-4	E-3F-1B-8-8	0.44	335	355	0.55	-2.76	0	1.35	3.2	
ANL-6-119-3	E-3F-1B-6-13	0.62	200	210	0.94	1.04	-0.3	2.00	3.3	
CP-6-4	E-3F-1B-13-11	0.68	700	750	7.82	11.8	60.1	23.09	44	
CP-6-2	E-3F-1B-13-6	0.79	700	750	12.3	16.0	92.0	29.30	53	
ANL-6-117-6	E-3F-1B-6-10	1.1	300	320	1.09	0.70	-0.9	2.97	2.8	
ANL-6-117-3	E-3F-1B-6-9	1.1	300	330	1.31	0.42	-1.1	2.14	2.1	
ANL-42-12-2	E-3F-1B-9-4	1.1	610	660	-	4.3	76.2	33.38	46	Irregularly swelled. in two pieces.
ANL-6-116-6	E-3F-1B-6-8	1.2	340	370	1.04	1.18	-0.6	2.97	2.6	
ANL-6-116-3	E-3F-1B-6-7	1.2	350	380	0.81	1.60	-0.7	2.94	2.6	
ANL-42-4-6	E-3F-1B-8-4	1.4	340	370	2.04	-2.64	-3.6	3.68	2.7	
CP-7-2	E-3F-1B-13-12	1.7	380	420	3.60	8.35	20.0	12.72	8.3	
ANL-6-115-6	E-3F-1B-6-6	2.0	500	540	3.85	2.58	0	17.26	10.0	Slight swelling near upper end.
ANL-42-14-2	E-3F-1B-8-12	2.4	490	530	3.16	5.24	119.4	15.52	7.7	Swelled near upper end.
ANL-42-2-6	E-3F-1B-8-2	2.4	560	610	1.77	4.15	-0.9	23.43	13	Slight swelling near upper end.
ANL-42-3-6	E-3F-1B-8-3	3.1	340	360	2.77	1.68	-1.2	12.48	4.6	
ANL-6-113-3	E-3F-1B-6-1	3.4	410	450	5.83	18.9	-10.6	24.55	10	Slight swelling near upper end.
ANL-6-113-6	E-3F-1B-6-2	3.8	480	510	-2.32	21.2	-26.4	25.82	9.2	Surface cracks.
ANL-42-19-2	E-3F-1B-9-11	5.0	650	700	18.8	13.2	-10.0	31.26	9.2	
ANL-42-1-6	E-3F-1B-8-1	5.3	640	690	3.29	78	-22.5	64.34	34	Severely swelled near upper end.
CP-9-2	E-3F-1A-1-11	5.5	740	790	6.67	43.7	25.2	52.50	20	
CP-9-6	E-3F-1A-1-8	5.8	720	760	11.4	37.5	-138.8	53.18	20	
CP-9-4	E-3F-1A-1-13	5.8	720	760	1.9	75	-494.0	54.72	21	
CP-8-6	E-3F-1A-1-12	5.8	630	670	b	b	b	59.48	25	In two pieces.
CP-8-2	E-3F-1A-1-10	6.2	640	680	b	b	b	59.83	23	In two pieces.
CP-8-1	E-3F-1A-1-9	6.2	640	680	b	b	b	60.28	24	Part of specimen not located.

[a]Calculated from the expression $\% \Delta \text{ Vol} = 100\left(\frac{\rho_i}{\rho_f} - 1\right)$, where ρ_i and ρ_f are the initial and final densities, respectively.

[b]Measurement not obtained.

TABLE VI. Effect of Irradiation on Unclad Specimens of U-6.7 wt % Fs-3.3 wt % Zr Alloy

Specimen No.	Original Specimen No.	Burnup, at. %	Midlength Irrad Temp, °C		Length Change, %	Avg Dia Change, %	Weight Change, mg	Density Decrease, %	% Δ Vol[a] at. % Burnup	Remarks
			Surface	Center						
CP-4-4	E-SF-2A-2-2	0.19	560	600	0.88	-1.04	-1.1	4.41	24	
CP-1-4	E-SF-2A-14-2	0.36	260	275	0.45	-0.76	24.4	1.03	2.8	
CP-2-6	E-SF-2A-2-1	0.45	285	305	0.50	0.21	0.2	1.30	2.9	
ANL-6-119-1	E-SF-2A-4-1	0.61	170	190	1.28	0.77	0.9	2.22	3.8	
CP-6-6	E-SF-2A-2-4	0.66	700	750	7.90	9.65	51.6	20.48	39	
ANL-42-10-4	E-SF-2A-2-5	1.1	440	470	1.94	0.48	0.1	3.40	3.1	
ANL-42-12-6	E-SF-2A-14-4	1.1	590	640	1.82	6.45	14.8	13.34	13	
ANL-6-116-1	E-SF-2A-1-2	1.2	320	350	0.82	0.90	-0.2	2.23	2.0	
ANL-42-15-5	E-SF-2A-14-7	1.4	250	270	1.03	3.34	-1.1	10.37	7.8	
ANL-42-22-4	E-SF-2A-1-10	1.4	340	360	2.07	1.11	-3.2	4.62	3.5	
ANL-42-9-3	E-SF-2A-14-1	1.5	560	610	1.60	0.84	-0.7	4.86	3.4	
ANL-42-23-5	E-SF-2A-1-12	1.5	360	390	2.30	0.55	-1.4	4.79	3.4	
ANL-42-24-6	E-SF-2A-1-13	1.7	350	380	2.10	0.69	-1.5	3.63	2.3	
ANL-42-14-4	E-SF-2A-14-6	2.3	390	420	3.21	2.44	-0.7	9.74	4.5	
ANL-42-16-6	E-SF-2A-14-8	2.7	410	450	5.74	34	3.5	33.71	19	Swelled near upper end.
ANL-42-18-4	E-SF-2A-14-10	3.1	320	350	2.30	2.02	-3.8	7.56	2.6	
ANL-6-123-4	E-SF-2A-1-7	3.7	420	460	12.3	50	-5.5	48.84	26	Swelled near upper end.
ANL-42-20-6	E-SF-2A-14-12	4.1	460	500	0.90	40	-1.1	45.66	21	Swelled near upper end.
ANL-42-19-5	E-SF-2A-14-11	4.8	540	580	8.72	20.2	6.0	29.19	8.6	

[a]Calculated from the expression $\% \Delta \text{ Vol} = 100\left(\frac{\rho_i}{\rho_f} - 1\right)$, where ρ_i and ρ_f are the initial and final densities, respectively.

TABLE VII. Effect of Irradiation on Unclad Specimens of U-10 wt % Fs-5 wt % Zr Alloy

Specimen No.	Original Specimen No.	Burnup, at. %	Midlength Irrad Temp, °C		Length Change, %	Avg Dia Change, %	Weight Change, mg	Density Decrease, %	% Δ Vol[a] at. % Burnup	Remarks
			Surface	Center						
CP-4-6	E-SF-1A-2-2	0.19	560	600	0.19	0.21	-7.6	b	-	
CP-1-3	E-SF-1A-8-8	0.36	260	275	0.33	2.82	1.6	0.23	2.0	
CP-2-2	E-SF-1A-2-1	0.45	310	355	0.14	0.14	-0.1	1.26	2.9	
ANL-6-119-4	E-SF-1A-1-4	0.63	160	170	0.34	0.83	-0.1	1.63	2.6	
ANL-42-13-6	E-SF-1A-8-5	0.65	310	340	0.17	1.52	1.3	5.85	9.7	
CP-6-3	E-SF-1A-2-3	0.73	700	750	1.50	2.42	7.2	5.12	7.6	
ANL-42-9-6	E-SF-1A-8-1	0.86	410	450	0.64	-0.03	3.3	2.98	3.6	
ANL-42-12-5	E-SF-1A-8-4	1.1	510	550	-0.31	5.41	5.0	7.69	7.6	
ANL-6-116-4	E-SF-1A-1-2	1.1	260	280	0.63	0.55	0.0	2.61	2.4	
ANL-42-15-4	E-SF-1A-8-7	1.4	220	240	1.72	2.35	0.0	5.64	4.2	
CP-7-6	E-SF-1A-2-4	1.4	350	390	-	0.41	b	8.61	6.5	In two pieces.
ANL-42-23-4	E-SF-1A-1-10	1.6	310	340	1.13	1.04	-3.1	4.91	3.2	
ANL-42-24-5	E-SF-1A-1-11	1.6	310	340	0.89	0.06	-3.8	2.46	1.7	
ANL-6-122-4	E-SF-1A-1-6	1.9	490	530	4.05	2.21	5.1	10.12	5.9	
ANL-42-16-5	E-SF-1A-1-12	2.6	370	400	6.58	51.7	1.8	42.84	27	Swelled near upper end.
ANL-42-17-6	E-SF-1A-8-9	2.7	380	410	5.12	3.81	-15.6	14.19	6.0	
ANL-42-20-5	E-SF-1A-8-12	3.9	400	430	4.82	4.79	-12.7	21.58	6.9	
ANL-42-19-4	E-SF-1A-8-11	4.6	460	500	6.77	6.60	b	17.6[c]	4.8[c]	
ANL-42-21-6	E-SF-1A-8-13	5.0	520	570	12.42	10.6	-59.0	27.25	7.6	

[a]Calculated from the expression $\% \Delta \text{ Vol} = 100\left(\frac{\rho_i}{\rho_f} - 1\right)$, where ρ_i and ρ_f are the initial and final densities, respectively.

[b]Measurement not obtained.

[c]Calculated from dimensional changes.

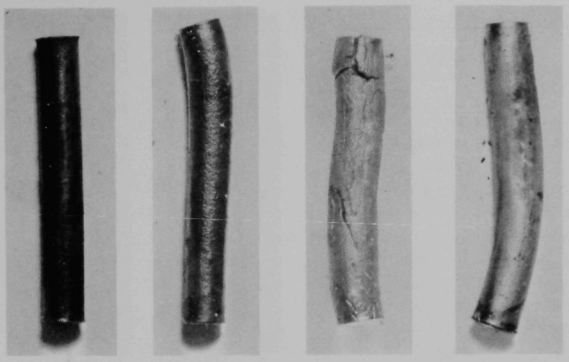

Specimen No.	ANL-42-10-6	ANL-42-14-6	ANL-6-113-4	ANL-42-19-3
Burnup, at. %	1.1	2.3	3.8	4.9
Max Irrad Temp, °C	520	410	530	650
% Δ Volume per at. % Burnup	4.3	9.9	12	9.3

Fig. 5. Postirradiation Condition of Typical U-3.3 wt % Fs-1.7 wt % Zr Alloy Specimens. Mag. 2X. Neg. Nos. MSD-26889, -27079, -27595, and -27449.

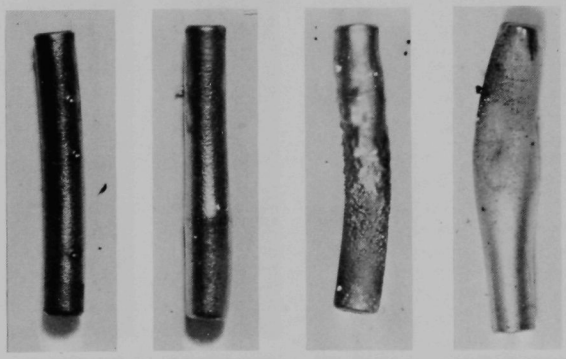

Specimen No.	ANL-42-10-5	ANL-42-14-5	ANL-6-113-1	ANL-42-19-6
Burnup, at. %	1.1	2.3	3.4	4.9
Max Irrad Temp, °C	520	430	460	680
% Δ Volume per at. % Burnup	3.0	11	7.4	17

Fig. 6. Postirradiation Condition of Typical U-3.7 wt % Fs Alloy Specimens. Mag. 2X. Neg. Nos. MSD-26888, -27078, -27592, and -27452.

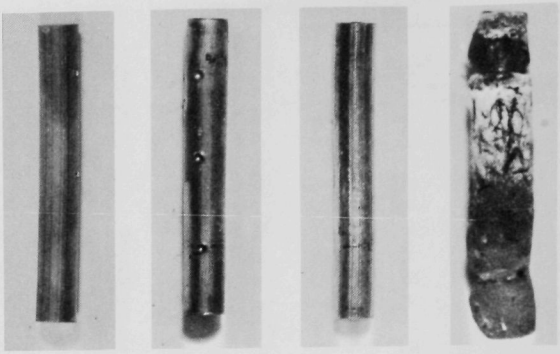

Specimen No.	ANL-6-116-5	ANL-42-14-1	ANL-42-7-6	CP-9-5
Burnup, at. %	1.2	2.4	3.7	5.8
Max Irrad Temp, °C	370	450	510	760
% Δ Volume per at. % Burnup	1.9	7.0	2.7	25

Fig. 7. Postirradiation Condition of Typical U-5 wt % Fs Alloy Specimens. Mag. 2X. Neg. Nos. MSD-24699, -27074, -27438, and -160663.

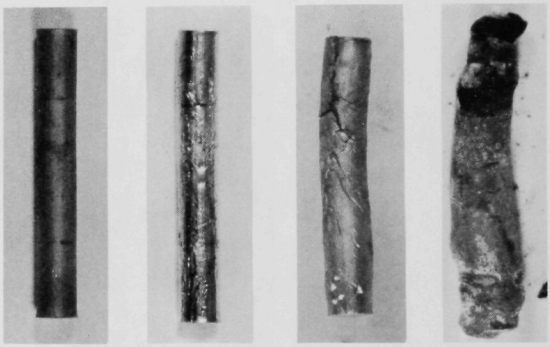

Specimen No.	ANL-6-116-3	ANL-42-3-6	ANL-6-113-6	CP-9-6
Burnup, at. %	1.2	3.1	3.8	5.8
Max Irrad Temp, °C	380	360	510	760
% Δ Volume per at. % Burnup	2.6	4.6	9.2	20

Fig. 8. Postirradiation Condition of Typical U-5 wt % Fs-2.5 wt % Zr Alloy Specimens. Mag. 2X. Neg. Nos. MSD-24697, -27701, -27598, and -160664.

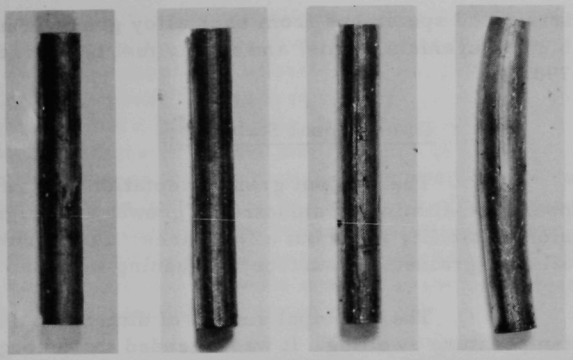

Specimen No.	ANL-6-116-1	ANL-42-14-4	ANL-42-18-4	ANL-42-19-5
Burnup, at. %	1.2	2.3	3.1	4.8
Max Irrad Temp, °C	350	420	350	580
% Δ Volume per at. % Burnup	2.0	4.5	2.6	8.6

Fig. 9. Postirradiation Condition of Typical U-6.7 wt % Fs-3.3 wt % Zr Alloy Specimens. Mag. 2X. Neg. Nos. MSD-24695, -27077, -27443, and -27451.

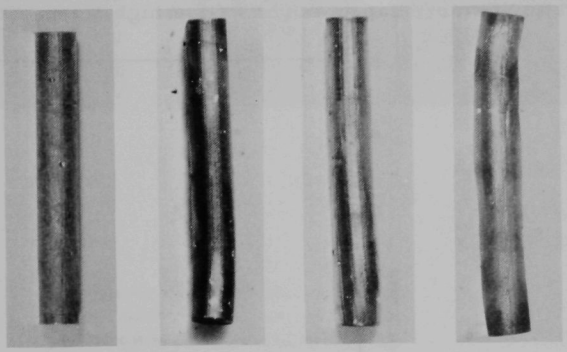

Specimen No.	ANL-6-116-4	ANL-42-17-6	ANL-42-19-4	ANL-42-21-6
Burnup, at. %	1.1	2.7	4.6	5.0
Max Irrad Temp, °C	280	410	500	570
% Δ Volume per at. % Burnup	2.4	6.0	4.8	7.6

Fig. 10. Postirradiation Condition of Typical U-10 wt % Fs-5 wt % Zr Alloy Specimens. Mag. 2X. Neg. Nos. MSD-24698, -27090, -27450, and -27591.

irradiated specimens from each alloy group. Burnups ranged as high as 6.2% of uranium atoms, and center fuel temperatures ranged from 170 to 790°C.

1. Dimensional Stability

The random grain orientation that resulted from the casting operation eliminated anisotropic growth as a significant source of dimensional stability in all but a few cases. Furthermore, the materials were all fine-grained, so surface roughening was also eliminated.

The principal source of dimensional instability was high-temperature swelling. It was intended that enough specimens would be irradiated under a wide range of experimental conditions to permit definition of the relationships between swelling rate, irradiation temperature, and burnup for each alloy. Unfortunately, the wide scatter in the experimental data did not permit quantitative conclusions to be drawn concerning the effects of irradiation temperature on swelling rates for most of the alloys. However, for the two alloys of greatest interest, U-5 wt % Fs and U-5 wt % Fs-2.5 wt % Zr, the general relationship between swelling rate and maximum irradiation temperature could be determined with reasonable certainty. Figure 11 shows the swelling curves for these two alloys. The U-5 wt % Fs alloy is more capable of resisting high-temperature irradiation swelling.

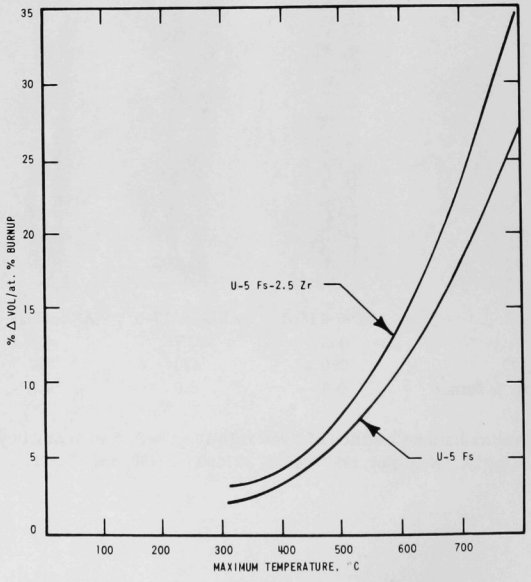

Fig. 11. Swelling Rates of U-5 wt % Fs and U-5 wt % Fs-2.5 wt % Zr Alloys under Irradiation. The curves are least-squares fits to the swelling data shown in Tables IV and V.

Several specimens exhibited a nonuniform type of swelling under irradiation, in which most of the volume changes developed at the upper ends of the specimens. Most of the specimens so affected had compositions known to be predominantly alpha-phase before irradiation. The upper-end swelling was usually in the form of a large bubble. Figure 12 shows a group of specimens in various stages of growth and collapse of a large bubble. Swelling at the upper ends of fuel specimens irradiated in NaK has been observed previously.[20-22] It is believed to be the result of local overheating due to temperature stratification at the top of the NaK surrounding the specimens. This condition, with its attendant temperature uncertainties, is believed to be largely responsible for the wide scatter in the data relating swelling rates of the alloys to irradiation temperature.

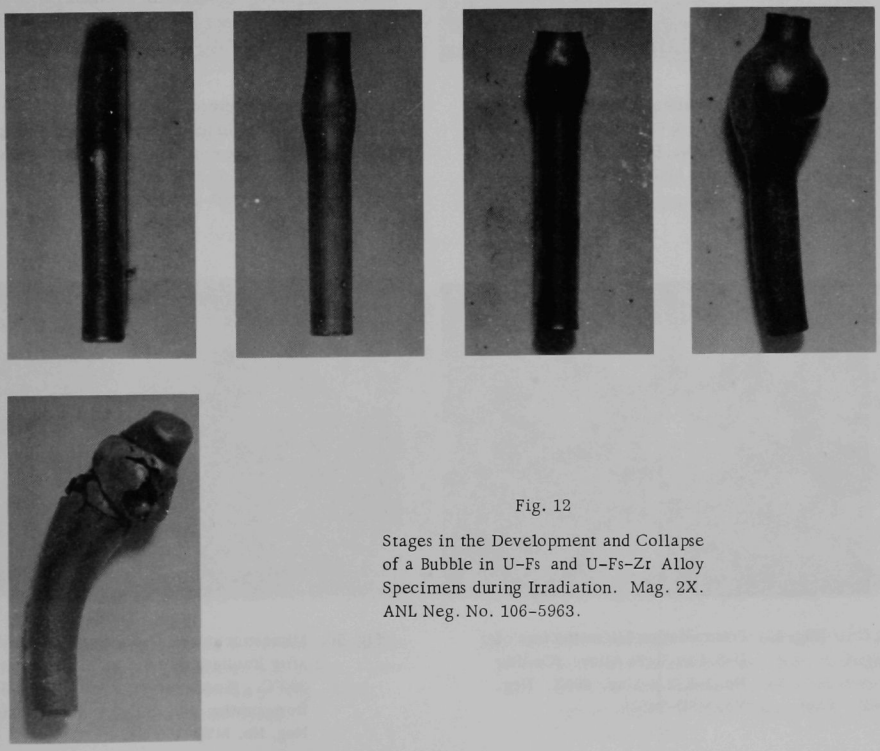

Fig. 12

Stages in the Development and Collapse of a Bubble in U-Fs and U-Fs-Zr Alloy Specimens during Irradiation. Mag. 2X. ANL Neg. No. 106-5963.

2. Microstructure

Figures 13-24 show photomicrographs of typical microstructures of the unirradiated and irradiated alloys investigated. In most cases, the unirradiated and irradiated specimens whose microstructures are shown are from the same casting.

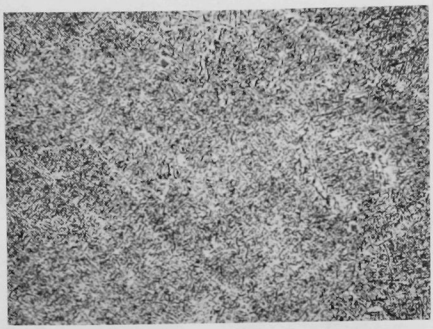

Fig. 13. Preirradiation Microstructure of U-3.3 wt % Fs-1.7 wt % Zr Alloy. (Casting No. E-3F-1C.) Mag. 400X. Neg. No. MSD-24929.

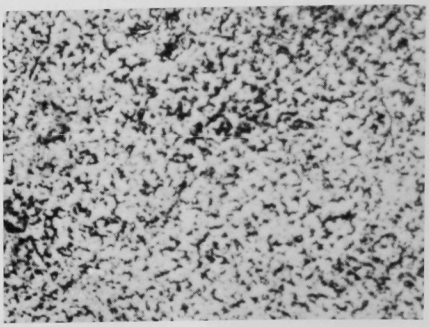

Fig. 14. Microstructure of U-3.3 wt % Fs-1.7 wt % Zr Alloy after Irradiation to 1.1 at. % Burnup at 520°C. (Specimen No. ANL-42-10-6 from casting No. E-3F-1C.) Mag. 400X. Neg. No. MSD-160665.

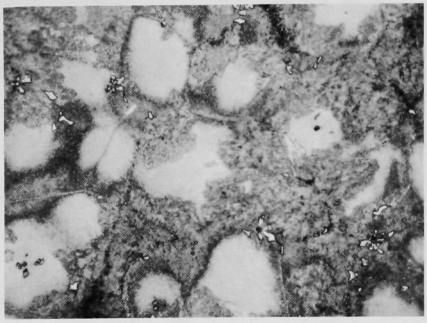

Fig. 15. Preirradiation Microstructure of U-3.7 wt % Fs Alloy. (Casting No. 1-E-2.) Mag. 400X. Neg. No. MSD-24930.

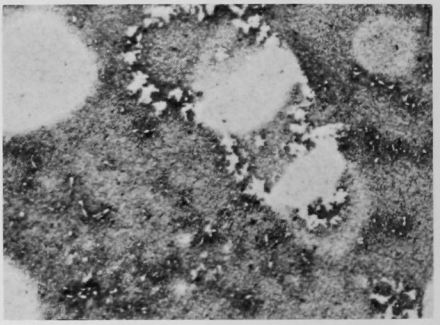

Fig. 16. Microstructure of U-3.7 wt % Fs Alloy after Irradiation to 3.1 at. % Burnup at 380°C. (Specimen No. ANL-42-18-5 from casting No. 1-E-2.) Mag. 400X. Neg. No. MSD-160666.

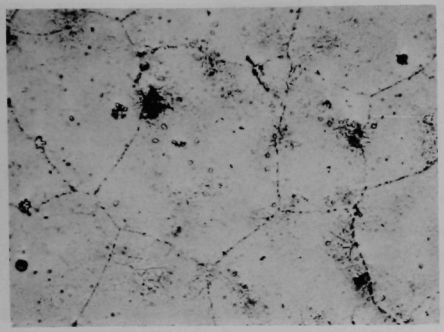

Fig. 17. Preirradiation Microstructure of U–5 wt % Fs Alloy. (Casting No. E-B16F-235.) Mag. 400X. Neg. No. MSD-24927.

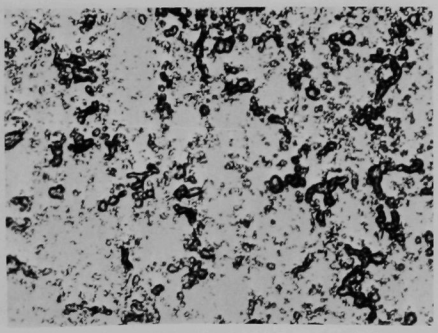

Fig. 18. Microstructure of U–5 wt % Fs Alloy after Irradiation to 1.2 at. % Burnup at 370°C. (Specimen No. ANL-6-116-5 from casting No. E-B16F-236.) Mag. 400X. Neg. No. MSD-28539.

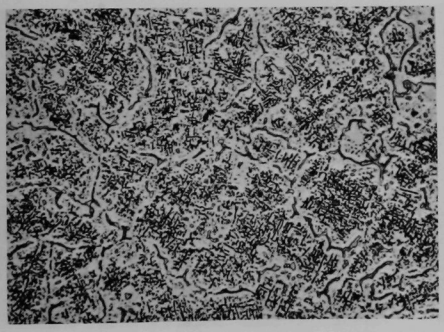

Fig. 19. Preirradiation Microstructure of U–5 wt % Fs–2.5 wt % Zr Alloy. Casting No. E-3F-1A.) Mag. 400X. Neg. No. MSD-24926.

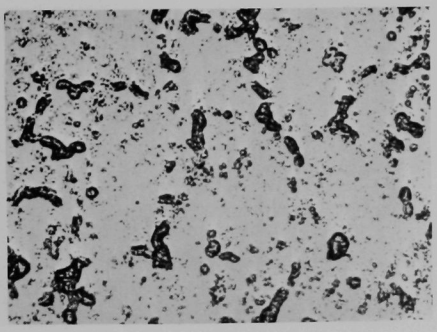

Fig. 20. Microstructure of U–5 wt % Fs–2.5 wt % Zr Alloy after Irradiation to 1.1 at. % Burnup at 320°C. (Specimen No. ANL-117-6 from casting No. E-3F-1B.) Mag. 400X. Neg. No. MSD-28543.

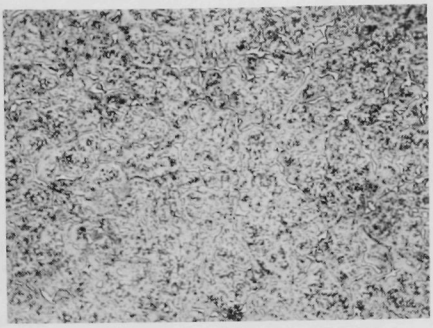

Fig. 21. Preirradiadiation Microstructure of U-6.7 wt % Fs-3.3 wt % Zr Alloy. (Casting No. E-SF-2A.) Mag. 400X. Neg. No. MSD-24931.

Fig. 22. Microstructure of U-6.7 wt % Fs-3.3 wt % Zr Alloy after Irradiation to 1.5 at. % Burnup at 390°C. (Specimen No. ANL-42-23-5 from casting No. E-SF-2A.) Mag. 400X. Neg. No. MSD-160667.

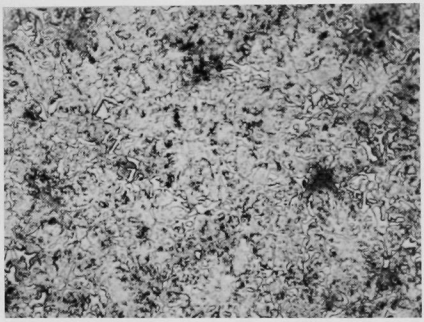

Fig. 23. Preirradiation Microstructure of U-10 wt % Fs-5 wt % Zr Alloy. (Casting No. E-SF-1A.) Mag. 400X. Neg. No. MSD-24928.

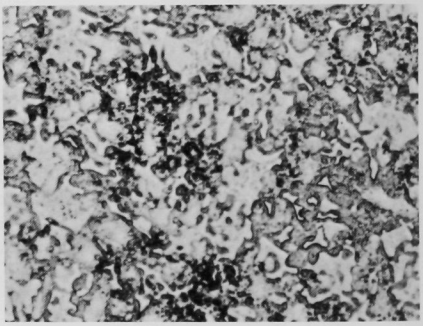

Fig. 24. Microstructure of U-10 wt % Fs-5 wt % Zr Alloy after Irradiation to 1.6 at. % Burnup at 340°C. (Specimen No. ANL-42-23-4 from casting No. E-SF-1A.) Mag. 400X. Neg. No. MSD-160668.

The irradiated specimens selected for metallographic studies were among those that did not show large volume changes. Their microstructures, therefore, were largely free of porosity of a size sufficient to be visible by optical metallography. All the specimens showed the general coarsening of structure and agglomeration of precipitated phases that are characteristic of uranium-base alloys irradiated to burnups greater than a few tenths of a percent. The effects of irradiation on the alloy microstructures did not appear to depend greatly on the alloy compositions.

More recently, electron-microscopic examinations at higher magnifications have been made on U-5 wt % Fs alloy from EBR-II driver fuel elements.[23] These examinations showed that swelling of the fuel at temperatures below 560°C occurs predominantly because of microtearing. Above 560°C, swelling is due to the formation and agglomeration of fission-gas bubbles. This behavior is similar to that observed for unalloyed uranium irradiated to burnups of several tenths of a percent.[23]

3. Phase Reversion

Because of the similarity of uranium-fissium alloys to the uranium-molybdenum alloy system, this investigation included experiments to determine whether fissium alloys irradiated at temperatures below the alpha-gamma transformation exhibited reversion to the gamma phase, as had been noted in comparable uranium-molybdenum alloys.[24] Such uranium-molybdenum alloys show the excellent dimensional stability characteristic of isotropic gamma-phase uranium. On the other hand, if the fission rate is too low to cause the alloy to revert to the gamma phase, a two-phase structure of alpha-plus-delta (or gamma) that shows enhanced swelling is formed.[25]

The experiments were therefore designed to determine if uranium-fissium material irradiated below the lower temperature boundary of the gamma phase (552°C) showed evidence of retained gamma phase. A sensitive test, measurement of electrical resistivity as a function of temperature, was used to determine whether the alloys were predominantly alpha or gamma. Uranium alloys that are predominantly gamma exhibit a negative temperature coefficient of resistivity. Uranium alloys that are predominantly alpha show a normal positive temperature coefficient.

Accordingly, to determine if the irradiation conditions induced phase reversion in the alloys, the electrical resistivity of unirradiated and irradiated specimens of each alloy (except the U-3.7 wt % Fs alloy) was measured at 17, -76, and -198°C with a Kelvin double bridge. At least two readings were taken on each specimen, and when the readings differed by more than 1 $\mu\Omega$, three or more readings were taken and averaged. For additional accuracy, each specimen was reversed in position in its holder and remeasured. The resistivity measurements at 17°C were made with the specimen immersed in chlorethane kept at constant temperature by

water circulating through coils in the bath. Mechanical stirrers were used to provide temperature uniformity. A mixture of isopropyl alcohol and dry ice was used for the measurements at -76°, and liquid nitrogen was used for the measurements at -198°C. Temperatures were measured with either mercury thermometers or copper-constantan thermocouples, depending on the temperature range of interest.

Figure 25 illustrates the effect of increasing fissium and zirconium content on the resistivity (ρ). The U-5 wt % Fs alloy is at least partially gamma phase. Increasing the alloy content increases the resistivity, as would be expected. It can also be noted from the slopes of the curves that increasing the fissium content tends to convert the alloys from alpha to gamma phase. Conversely, zirconium tends to stabilize the alpha

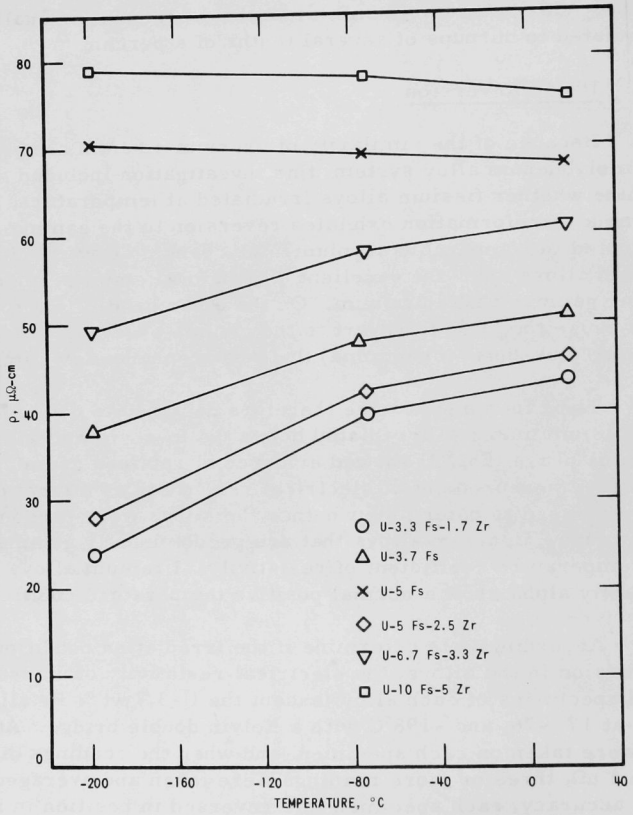

Fig. 25. Electrical Resistivity vs Temperature of Unirradiated U-Fs and U-Fs-Zr Alloys

phase. Both of these effects confirm earlier results of metallographic examinations made during studies of phase relations in the uranium-fissium-zirconium system.[12]

Table VIII and Figs. 26-30 show the effects of irradiation on all the alloys studied except U-3.7 wt % fissium, for which a suitable specimen was not available. The changes in electrical resistivity induced by irradiation were greatest for the specimens with lower alloy contents. Figure 27 shows that irradiation of the U-5 wt % Fs alloy transformed the retained gamma into the thermodynamically stable alpha phase. (The slope of the resistivity curve changed from negative to positive with irradiation.) It can be concluded that uranium-fissium alloys do not exhibit reversion to the gamma phase under at least the range of conditions studied in this experiment.

TABLE VIII. Effect of Irradiation on Electrical Resistivity of U-Fs and U-Fs-Zr Alloys

Specimen No.	Composition, wt %	Burnup, at. %	Max Irrad Temp, °C	Test Temp, °C	ρ, μΩ-cm	Avg ρ/°C	Irradiation-induced Change in Avg ρ/°C, %
-	U-3.3 Fs-1.7 Zr	None	-	15	40	0.090	
				-75	33		
				-197	21		
ANL-6-117-4	U-3.3 Fs-1.7 Zr	1.2	410	12	56	0.071	-21
				-68	51		
				-198	41		
-	U-5 Fs	None	-	16	66	-0.0093	
				-77	67		
				-197	68		
ANL-6-116-5	U-5 Fs	1.2	370	13	52	0.090	1100
				-74	46		
				-198	33		
-	U-5 Fs-2.5 Zr	None	-	16	46	0.094	
				-75	39		
				-197	26		
ANL-6-119-3	U-5 Fs-2.5 Zr	0.62	210	12	57	0.052	-45
				-73	55		
				-198	46		
ANL-6-117-6	U-5 Fs-2.5 Zr	1.1	320	12	57	0.071	-24
				-72	52		
				-198	42		
ANL-6-117-3	U-5 Fs-2.5 Zr	1.1	330	13	53	0.076	-19
				-72	49		
				-198	37		
ANL-6-116-6	U-5 Fs-2.5 Zr	1.2	370	13	53	0.095	1.1
				-71	46		
				-198	33		
ANL-6-116-3	U-5 Fs-2.5 Zr	1.2	380	13	48	0.081	-14
				-72	44		
				-198	31		
-	U-6.7 Fs-3.3 Zr	None	-	14	55	0.066	
				-74	51		
				-198	41		
ANL-6-119-1	U-6.7 Fs-3.3 Zr	0.61	190	12	63	0.062	-6.1
				-70	59		
				-198	50		
-	U-10 Fs-5 Zr	None	-	16	73	0.0047	
				-77	73		
				-197	72		
ANL-6-119-4	U-10 Fs-5 Zr	0.63	170	12	74	0.0095	100
				-71	74		
				-198	72		
ANL-6-116-4	U-10 Fs-5 Zr	1.1	280	13	73	0.024	410
				-74	72		
				-198	68		

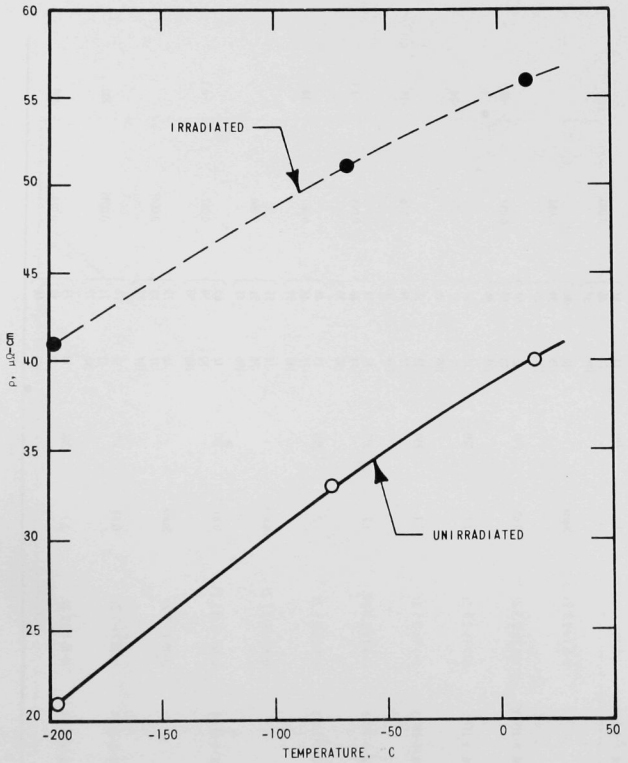

Fig. 26. Effect of Irradiation to 1.2 at. % Burnup at 410°C on the Electrical Resistivity of U-3.3 wt % Fs-1.7 wt % Zr Alloy

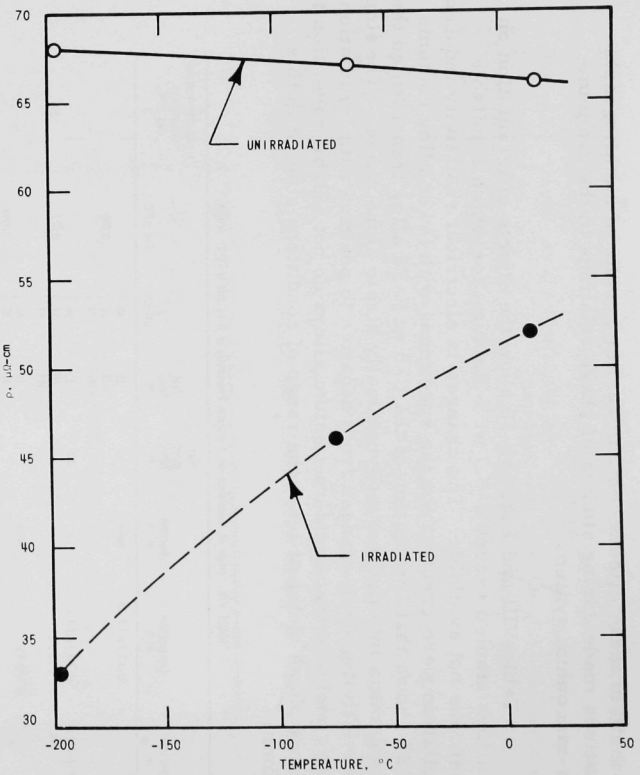

Fig. 27. Effect of Irradiation to 1.2 at. % Burnup at 370°C on the Electrical Resistivity of U-5 wt % Fs Alloy

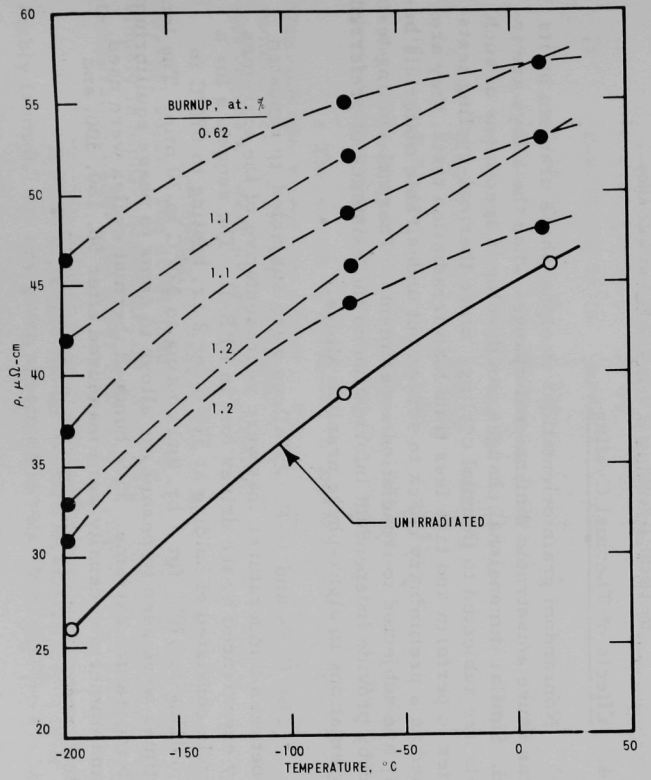

Fig. 28. Effect of Irradiation at Temperatures from 210 to 380°C on the Electrical Resistivity of U-5 wt % Fs-2.5 wt % Zr Alloy

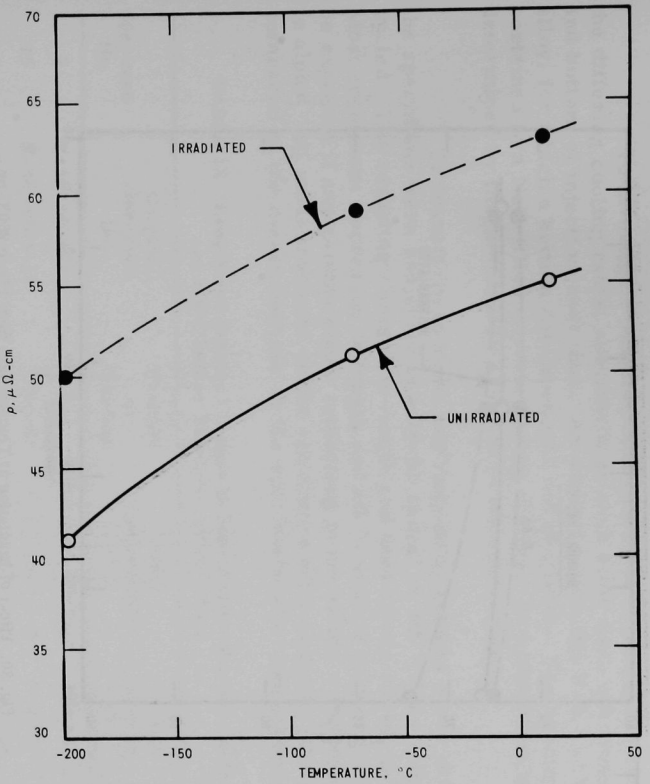

Fig. 29. Effect of Irradiation to 0.61 at. % Burnup at 190°C on the Electrical Resistivity of U-6.7 wt % Fs-3.3 wt % Zr Alloy

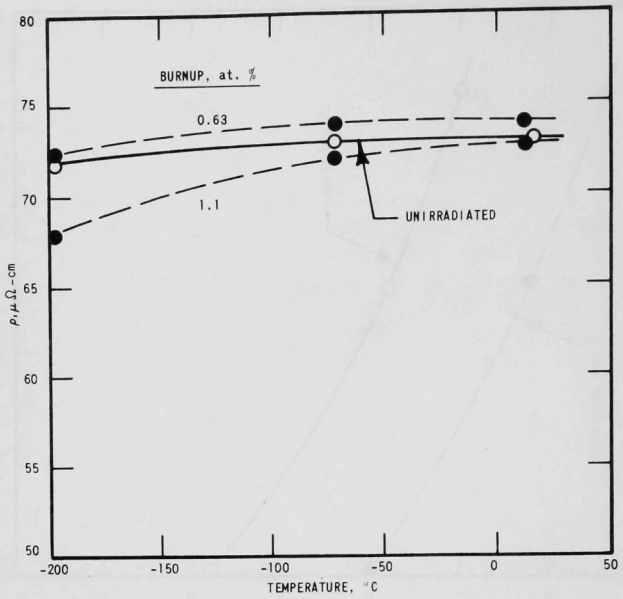

Fig. 30. Effect of Irradiation at Temperatures from 170 to 280°C on the Electrical Resistivity of U-10 wt % Fs-5 wt % Zr Alloy

4. Effects of Thermal Cycling

Nonrandom grain orientations in alpha-phase uranium or its alloys can cause anisotropic dimensional changes when the alloys are irradiated. Similar dimensional changes can develop if specimens of such materials are subjected to thermal cycling. Since thermal-cycling tests are easier to perform and take less time than irradiation tests, they are often used as a preliminary check to screen out undesirable materials before they are subjected to irradiation experiments. Thermal-cycling tests can thereby provide independent information on the existence of preferred grain orientations in alpha-phase uranium alloys.

The U-Fs and U-Fs-Zr alloys were subjected to repeated cycling between temperatures that were representative of the extremes normally experienced by the driver fuel in EBR-II. The sequence for a single cycle consisted of holding at 370°C for 2 hr, heating to 670°C in 30 min, holding at 670°C for 1 hr, and cooling to 370°C in 30 min. The long holding times were used to permit the alloys to come to phase equilibrium at each temperature extreme. Five hundred thermal cycles were used. Length and immersion density were measured after 58, 150, 300, and 500 cycles.

To investigate possible differences in behavior resulting from the differing cooling rates, specimens of each alloy were cut from the top and bottom of injection-cast pins. An exception was the U-3.7 wt % Fs alloy, for which a bottom specimen was not available. The specimens were contained in a NaK-filled capsule during cycling. Temperatures were determined by thermocouples adjacent to the specimens.

To transform to alpha any remaining gamma phase in the alloys, the specimens were subjected to a 24-hr anneal at 500°C before they were cycled. The resulting changes in length and density are shown in Table IX. Most specimens decreased in length and all increased in density, as would be expected if any gamma phase remaining in the alloys were transformed to alpha. All measurements on the specimens after thermal cycling were compared to the measurements on the specimens after the anneal.

TABLE IX. Length and Density Changes of Specimens Annealed for 24 hr at 500°C before Thermal-cycling Tests

Specimen No.	Original Specimen No.	Position in Casting	Alloy Composition, wt %	Length Change, %	Density Change, %
9	E-3F-1C-6-1	Top	U-3.3 Fs-1.7 Zr	0.00	0.64
15	E-3F-1C-6-13	Bottom	U-3.3 Fs-1.7 Zr	-0.15	0.67
13	1E2-4-13	Bottom	U-3.7 Fs	0.039	0.69
11	E-B16F-235-14-1	Top	U-5 Fs	-0.020	1.16
17	E-B16F-235-14-13	Bottom	U-5 Fs	-0.094	0.72
8	E-3F-1A-3-1	Top	U-5 Fs-2.5 Zr	0.00	0.71
14	E-3F-1A-3-13	Bottom	U-5 Fs-2.5 Zr	-0.054	0.81
7	E-SF-2A-3-1	Top	U-6.7 Fs-3.3 Zr	-0.52	0.34
12	E-SF-2A-3-13	Bottom	U-6.7 Fs-3.3 Zr	-0.22	1.01
10	E-SF-1A-5-1	Top	U-10 Fs-5 Zr	-0.12	N.A.
16	E-SF-1A-5-13	Bottom	U-10 Fs-5 Zr	-0.34	0.98

The effects of thermal cycling on the length and density of the annealed specimens are shown in Figs. 31 and 32, respectively. Table X summarizes the effects. Elongations of up to 1.42% were noted, and density decreases were as large as 1.63%.

The density decreases are believed to be due to formation of internal voids. The development of internal voids has been observed previously in alpha-phase uranium alloys that have been thermally cycled to temperatures above the upper boundary of single-phase alpha.[26]

A ratio of length change to density change that differs appreciably from 0.7 for any given specimen in this study indicates that some

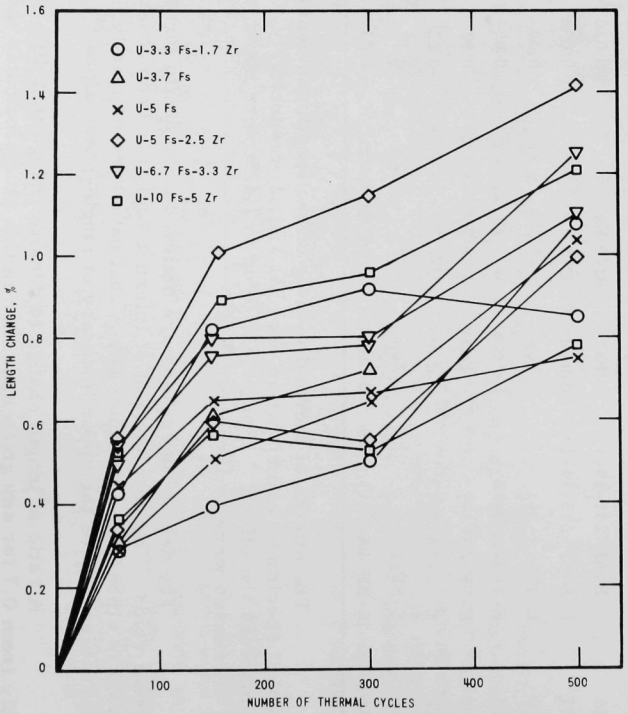

Fig. 31. Cumulative Changes in Length of U-Fs and U-Fs-Zr Alloy Specimens Cycled between 370 and 670°C

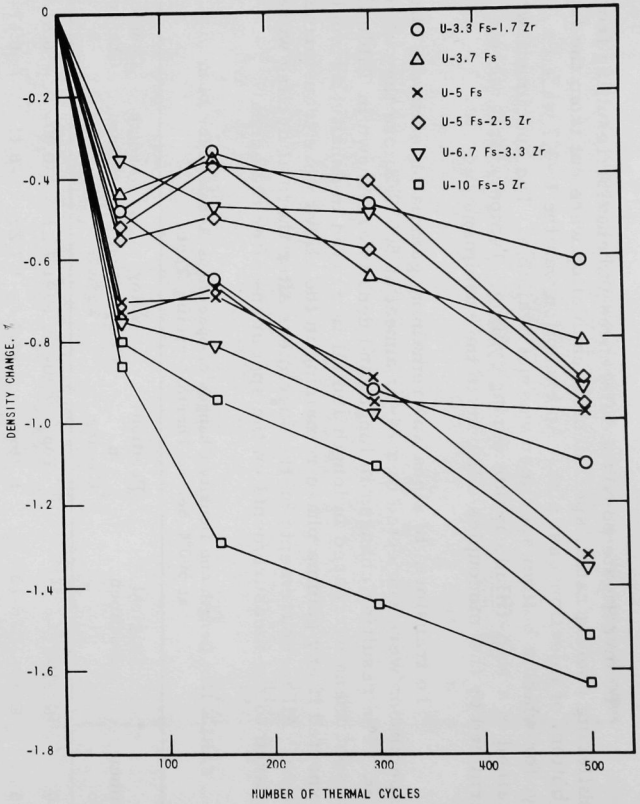

Fig. 32. Cumulative Changes in Density of U-Fs and U-Fs-Zr Alloy Specimens Cycled between 370 and 670°C

TABLE X. Summary of Cumulative Changes in Length (L) and Density (D) of U-Fs and U-Fs-Zr Alloy Specimens Cycled between 370 and 670°C

Specimen No.	Original Specimen No.	Position in Casting	Alloy Composition, wt %	Total Number of Cycles							
				58		150		300		500	
				% ΔL	% ΔD	% ΔL	% ΔD	% ΔL	% ΔD	% ΔL	% ΔD
9	E-3F-1C-6-1	Top	U-3.3 Fs-1.7 Zr	0.29	-0.48	0.39	-0.34	0.51	-0.47	1.08	-0.61
15	E-3F-1C-6-13	Bottom	U-3.3 Fs-1.7 Zr	0.43	-0.48	0.82	-0.65	0.92	-0.92	0.85	-1.11
13	1E2-4-13	Bottom	U-3.7 Fs	0.31	-0.44	0.61	-0.35	0.72	-0.64	N.A.	-0.81
11	E-B16F-235-14-1	Top	U-5 Fs	0.44	-0.74	0.65	-0.67	0.66	-0.95	0.75	-0.98
17	E-B16F-235-14-13	Bottom	U-5 Fs	0.30	-0.71	0.51	-0.68	0.64	-0.89	1.05	-1.33
8	E-3F-1A-1	Top	U-5 Fs-2.5 Zr	0.34	-0.52	0.61	-0.36	0.55	-0.41	1.00	-0.90
14	E-3F-1A-13	Bottom	U-5 Fs-2.5 Zr	0.56	-0.55	1.01	-0.50	1.15	-0.58	1.42	-0.97
7	E-SF-2A-3-1	Top	U-6.7 Fs-3.3 Zr	0.49	-0.36	0.76	-0.47	0.78	-0.48	1.25	-0.91
12	E-SF-2A-3-13	Bottom	U-6.7 Fs-3.3 Zr	0.56	-0.75	0.80	-0.81	0.80	-0.98	1.10	-1.35
10	E-SF-1A-5-1	Top	U-10 Fs-5 Zr	0.34	-0.86	0.57	-1.29	0.53	-1.44	0.78	-1.63
16	E-SF-1A-5-13	Bottom	U-10 Fs-5 Zr	0.55	-0.80	0.90	-0.96	0.96	-1.11	1.21	-1.52

degree of preferred grain orientation is present. This appears to be the case for specimens of the alloys that were predominantly alpha phase in the as-cast condition, i.e., U-3.3 wt % Fs-1.7 wt % Zr, U-3.7 wt % Fs, U-5 wt % Fs-2.5 wt % Zr, and the U-6.7 wt % Fs-3.3 wt % Zr specimen from the upper end of the casting.

5. Effects of Postirradiation Heating

An irradiated specimen of each alloy was progressively subjected to a series of anneals at elevated temperatures (400-775°C) to obtain additional information on the influence of temperature on swelling behavior.[27] The specimens were annealed in high-purity argon for 24 hr at each temperature. Heating was provided by a platinum-wound furnace whose temperature was controlled within ±5°C. After each annealing treatment, the specimens were cooled to room temperature and measured for changes in length, diameter, and immersion volume. The specimens were sectioned and examined metallographically after the final anneal. Table XI shows the preannealing irradiation history of the specimens.

TABLE XI. Irradiation History of Specimens Subjected to Postirradiation Annealing Tests

Specimen No.	Original Specimen No.	Alloy Composition, wt %	Burnup, at. %	Midlength Irrad Temp, °C	
				Surface	Center
ANL-42-10-6	E-3F-1C-8-2	U-3.3 Fs-1.7 Zr	1.1	470	520
ANL-42-18-5	1E2-12-10	U-3.7 Fs	3.1	350	380
ET-3-14-5[a]	-	U-5 Fs	1.5	N.A.	370
ET-2-2-5[a]	-	U-5 Fs-2.5 Zr	1.0	N.A.	280
ANL-42-23-5	E-SF-2A-14-7	U-6.7 Fs-3.3 Zr	1.4	250	270
ANL-42-23-4	E-SF-1A-1-10	U-10 Fs-5 Zr	1.6	310	340

[a]Specimens taken from a different series of irradiation experiments than those described in this report. However, they were manufactured and irradiated under the same conditions as the specimens described in this report.

Figure 33 summarizes the volume changes per at. % burnup measured for each specimen as a function of annealing temperature. Length and diameter changes showed similar trends. As expected, the composition with the lowest alloy content showed the onset of severe swelling at the lowest temperature (500-525°C). This alloy, however, showed the lowest swelling/burnup ratio of any of the six compositions tested. The most severe swelling in the range 575-650°C was shown by the U-5 wt % Fs alloy.

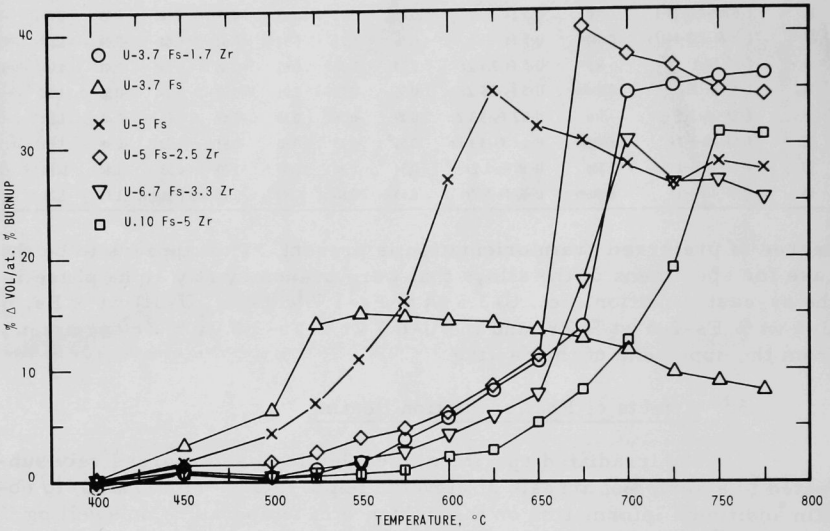

Fig. 33. Effect of Successive 24-hr Anneals on the Volume of Irradiated U-Fs and U-Fs-Zr Alloys

With the exception of the U-3.3 wt % Fs-1.7 wt % Zr composition, all alloys steadily decreased in volume after annealing at temperatures above that at which the most rapid swelling was observed. This temperature also produced severe surface cracking in all specimens. The cracks enlarged and deepened with each subsequent anneal. Presumably, the cracking was accompanied by bubble linkup within the specimens, which permitted most of the retained fission gas to be released. Other postirradiation heating tests on uranium-fissium alloys have shown that rapid release of fission gas coincides with the onset of severe swelling.[28]

The metallographic sections of the specimens showed that all had developed extensive, uniformly distributed porosity. In addition, the U-Fs specimen had developed a large central void (see Fig. 34). This void is believed to have caused much of the volume increase indicated in Fig. 33.

B. Clad Specimens

The irradiations of the U-5 wt % Fs and U-5 wt % Fs-2.5 wt % Zr alloys included experiments intended to determine the behavior of the alloys

Fig. 34. Transverse Section of Irradiated U-5 wt % Fs Alloy Specimen after Annealing at Temperatures up to 775°C. Mag. 20X. Neg. No. MSD-160601.

when irradiated with cladding restraint. Several different cladding materials were used. They were selected on the basis of their intended use in a planned subsequent series of irradiations on U-Pu-Fs alloys.[8,9] The cladding materials used in the experiments reported here included niobium, vanadium, V-10 wt % Ti-3 wt % Nb alloy, yttrium, and Inconel-X. The latter material was procured in the solution-treated condition and was separated from the fuel by a 0.001-in.-thick zirconium foil to avoid possible eutectic formation between the fuel and cladding.

All the clad specimens were irradiated for 10-13 months in the CP-5 reactor in instrumented temperature-controlled capsules of the type shown in Fig. 4. Chromel-Alumel thermocouples with an outer sheath diameter of 0.020 in. were prepared at ANL and used for measuring central fuel temperature in some of the specimens. These small-diameter thermocouples were used to reduce local temperature perturbations. The remaining thermocouples, also Chromel-Alumel, in the capsule were commercially procured and had a 1/16-in.-dia sheath. Controlled temperatures were achieved by resistance heaters, with ratings up to 3 kW, submerged in the NaK.

The specimens were 2-in.-long lengths of injection-cast fuel pins. They were inserted in cladding having the same dimensions as those used for the EBR-II fuel element (0.174-in. OD, 0.009-in. wall thickness). The cladding was sealed at the bottom, but was left open at the top to permit capsule NaK to enter the fuel-cladding annulus and to simplify insertion of thermocouples into the center of the fuel pins. Four vent holes, two each at different elevations, were also located near the bottom of the cladding to facilitate entry of NaK into the annulus. Entry of NaK and wetting of the interfaces were ensured by vibrating the capsules for 2 hr at 400°C.

1. Dimensional Stability

Table XII summarizes the results of the irradiations of clad specimens of U-5 wt % Fs and U-5 wt % Fs-2.5 wt % Zr alloys. Fuel burnups as high as 5.8 at. % were achieved at center fuel temperatures up to 700°C.

TABLE XII. Effects of Irradiation on Clad Specimens of U-5 wt % Fs and U-5 wt % Fs-2.5 wt % Zr Alloy

Specimen No.	Original Specimen No.	Fuel Composition, wt %	Cladding Material	Burnup, at. %	Max Fuel Temp, °C	Max Cladding Temp, °C	Fuel Length Change, %	Max Cladding Diameter Change, %	Remarks
CP-14-2	E-B16F-235-13-4	U-5 Fs	Niobium	5.3	700	600	4.8	0.56	Specimen intact, straight. Fuel extrusions up to 30 mm long from vent holes.
CP-13-2	E-B16F-235-13-3	U-5 Fs	Niobium	5.8	700	600	15.5	1.40	Specimen intact, slightly curved. Fuel extrusions 10 mm long from vent holes.
CP-14-3	E-B16F-235-13-6	U-5 Fs	Vanadium	5.3	700	600	9.8	1.40	Specimen intact, straight. Fuel extrusions up to 18 mm long from vent holes.
CP-13-3	E-B16F-235-13-5	U-5 Fs	Vanadium	5.8	700	600	2.8	1.50	Cladding split 9 mm long. Fuel extrusions up to 8 mm long from vent holes and cladding split.
CP-14-1	E-B16F-235-13-2	U-5 Fs	Yttrium	5.3	700	600	2.4	45	Cladding split 50 mm long. Specimen uniformly swelled.
CP-13-1	E-B16F-235-13-1	U-5 Fs	Yttrium	5.8	700	600	-5.4	87	Cladding split 50 mm long. Specimen uniformly swelled.
CP-15-2	E-3F-1A-6-2	U-5 Fs-2.5 Zr	Niobium	4.8	650	560	-3.8	1.70	Specimen intact, straight. Fuel extrusions 3 mm long from vent holes.
CP-15-5	E-3F-1A-6-4	U-5 Fs-2.5 Zr	Vanadium	4.7	610	525	-2.2	2.86	Specimen intact, curved. Fuel extrusions 4 mm long from vent holes.
CP-15-3	E-3F-1A-7-1	U-5 Fs-2.5 Zr	Vanadium	4.8	650	560	-11.2	1.03	Cladding split 9 mm long. Fuel extrusions 4 mm long from vent holes and cladding split.
CP-15-4	E-3F-1A-6-3	U-5 Fs-2.5 Zr	V-10 wt % Ti-3 wt % Nb	4.7	610	525	-1.19	0.74	Specimen intact, straight. Fuel extrusions 3 mm long from vent holes.
CP-15-6	E-3F-1A-7-2	U-5 Fs-2.5 Zr	Inconel-X	4.7	610	525	-	45	Specimen fractured in two pieces. Numerous brittle cladding failures. Fuel extrusions 2 mm long from vent holes.
CP-15-1	E-3F-1A-6-1	U-5 Fs-2.5 Zr	Inconel-X	4.8	650	560	2.9	20	Numerous brittle cladding failures. Fuel extrusions 2 mm long from vent holes.

Fuel swelling in all specimens caused extrusion of the fuel alloy from the vent holes in the lower part of the cladding (except those specimens clad in yttrium). Figure 35 shows a typical example of such fuel extrusions, one of which is ~0.4 in. long. Other specimens developed fuel extrusions from the cladding vent holes that would have been over an inch long if they could have been recovered intact.

Interestingly, except for specimen CP-13-2, no fuel pin elongated appreciably within its cladding. This was true even though the upper end of the cladding was open on all specimens and some specimens had no central thermocouples that might have provided some degree of axial restraint. Apparently, frictional forces between the fuel and cladding prevent any appreciable axial movement of the fuel within the cladding.

No failures of the niobium or the V-10 wt % Ti-3 wt % Nb cladding occurred.

Two of the four vanadium claddings developed failures. Each failure was a ~0.3-in.-long ductile split near the center of the specimen. A characteristic wedge-shaped extrusion of fuel then occurred through the defect, as shown in Fig. 36.

Both yttrium-clad specimens developed severe cladding failures. The failures are surmised to have developed early. This conclusion is based on the extensive swelling of the fuel and on the absence of fuel extrusions from the cladding vent holes. Figure 37 shows the yttrium-clad specimen with the higher burnup.

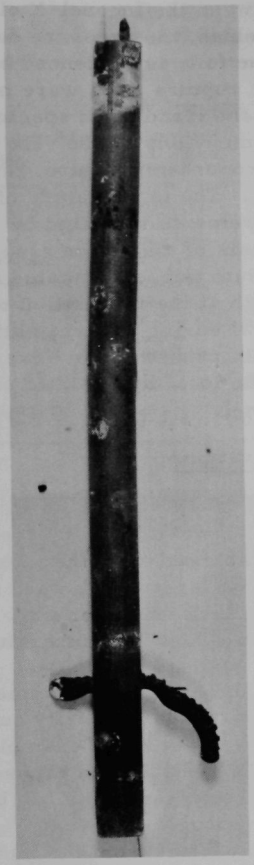

Fig. 35

Specimen No. CP-13-2, Niobium-clad U-5 wt % Fs Alloy, after 5.8 at.% Burnup at Central Fuel Temperature of 700°C. Sheathed fuel thermocouple protrudes from top of specimen. Fuel has extruded through the four vent holes in the cladding. Mag. 2X. Neg. No. MSD-160604.

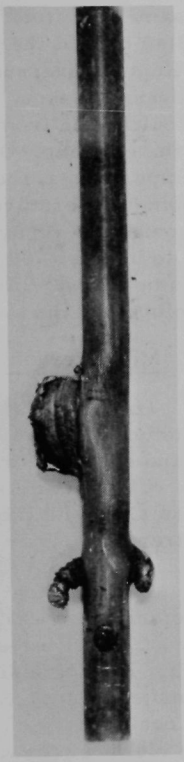

Fig. 36

Specimen No. CP-15-3, Vanadium-clad U-5 wt % Fs-2.5 wt % Zr Alloy, after 4.8 at. % Burnup at Central Fuel Temperature of 650°C. Fuel is protruding from both a split in the cladding and the vent holes. Mag. 2X. Neg. No. MSD-160606.

Fig. 37

Specimen No. CP-13-1, Yttrium-clad U-5 wt % Fs Alloy, after 5.8 at. % Burnup at Central Fuel Temperature of 700°C. Cladding failure is believed to have occurred early in the experiment, as evidenced by the absence of fuel extrusions from the cladding vent holes. Mag. 2X. Neg. No. MSD-160603.

Both specimens clad with Inconel-X developed cladding failures with a highly brittle appearance. The specimen with the higher burnup is shown in Fig. 38. The Inconel-X tubing used for the cladding had been procured in the ductile solution-treated condition, as stated earlier. Postirradiation bend tests attempted on cladding fragments from specimen CP-15-1 confirmed the brittle condition of the cladding.

The 0.001-in.-thick zirconium foil between the Inconel-X cladding and the fuel covered the vent holes. Nevertheless, the pressure developed by the swelling fuel eventually ruptured the foil, as evidenced by the extrusion of fuel from the vent holes. Hydrostatic rupture tests were made on several samples of the same foil stock used in the irradiation specimens. The backup plate had a drilled hole of the same dimensions as the vent holes in the specimen cladding. Rupture pressures, at room temperature, ranged from 1200 to 1850 psi and averaged about 1475 psi. The temperature of the foil during irradiation was calculated from measurements indicated by thermocouples adjacent to the cladding. On the basis of the known properties of zirconium at elevated temperatures, the zirconium foil is estimated to have retained 48% of its room-temperature strength at the irradiation temperature. The pressure required to rupture the foil during the irradiation test is therefore estimated to be near 700 psi. This pressure can be assumed to be a lower limit for the local hydrostatic pressures developed by the swelling fuel.

2. Metallographic Observations

The six intact specimens with claddings of niobium, vanadium, and V-10 wt % Ti-3 wt % Nb alloy were sectioned and examined metallographically. Both the fuel alloys U-5 wt % Fs and U-5 wt % Fs-2.5 wt % Zr were represented, as shown in Table XIII. Each specimen was sectioned transversely at the point of highest temperature.

The metallographic section of each specimen was characterized by a central zone of high porosity surrounded by a zone of lesser porosity. A typical example is shown in Fig. 39. Pore sizes in the central zone ranged up to approximately 120 μ. Some of the larger pores had been formed by coalescence of smaller pores, as shown in Fig. 40. The zone of high porosity was slightly offset from the central axis of the specimen because of the radial temperature profile in the three-specimen capsule arrangement.

Most of the specimens showed evidence of reaction between the fuel and the cladding. Reaction layers were formed by U-5 wt % Fs alloy with niobium and vanadium cladding to depths up to 3.7 mils. Typical reaction zones are shown in Figs. 41 and 42. Cracks of the type shown in Fig. 42 were also noted in the niobium-clad U-5 wt % Fs alloy.

Fig. 38. Specimen No. CP-15-1, Inconel-X-clad U-5 wt % Fs-2.5 wt % Zr Alloy, after 4.8 at. % Burnup at Central Fuel Temperature of 650°C. Cladding failed in a characteristically brittle manner. Mag. 2X. Neg. No. MSD-160605.

TABLE XIII. Results of Microscopic Measurements on Transverse Sections of Jacketed U-Fs Alloy

Specimen No.	Fuel Composition, wt %	Cladding Material	Max Void Size, μ	Depth of Fuel/Cladding Reaction Zone, mils
13-2	U-5 Fs	Niobium	30	None
14-2	U-5 Fs	Niobium	120	3.7
14-3	U-5 Fs	Vanadium	100	3.6
15-2	U-5 Fs-2.5 Zr	Niobium	46	6.1
15-4	U-5 Fs-2.5 Zr	V-10 wt % Ti-3 wt % Nb	64	1.5
15-5	U-5 Fs-2.5 Zr	Vanadium	28	1.4

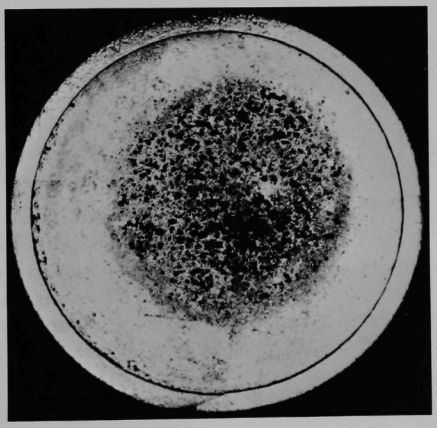

Fig. 39

Transverse Section of Specimen No. 14-3, Vanadium-Clad U-5 wt % Fs Alloy, after 5.3 at. % Burnup at Central Fuel Temperature of 700°C. Mag. 17X. ANL Neg. No. 106-6788.

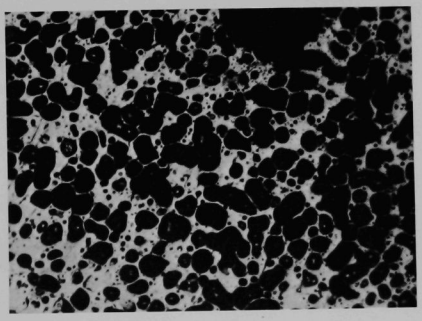

Fig. 40

Pore Coalescence in U-5 wt % Fs Alloy Irradiated to 5.3 at. % Burnup at 700°C. (Specimen No. CP-14-2.) Mag. 200X. Neg. No. MSD-160607.

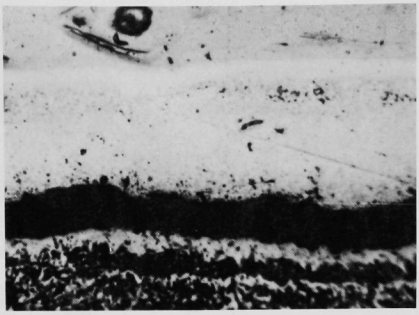

Fig. 41

Typical Reaction Zone between U-5 wt % Fs Alloy and Niobium Cladding. (Specimen No. 14-2.) Mag. 400X. Neg. No. MSD-160608.

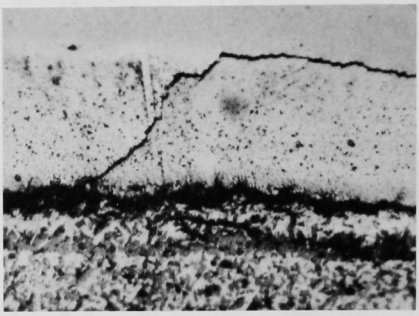

Fig. 42

Typical Reaction Zone between U-5 wt % Fs Alloy and Vanadium Cladding. (Specimen No. 14-3.) Mag. 400X. Neg. No. MSD-160612.

The U-5 wt % Fs-2.5 wt % Zr alloy showed more extensive reaction with niobium (see Fig. 43). Reaction zones as thick as 6 mils were noted, only about 5 of the original 9 mils of cladding thickness remaining unaffected. The layers were firmly attached to the fuel and cladding, as evidenced by the fracture pattern shown in Fig. 44. Only slight reaction occurred with vanadium and V-10 wt % Ti-3 wt % Nb alloy cladding (see Figs. 45 and 46).

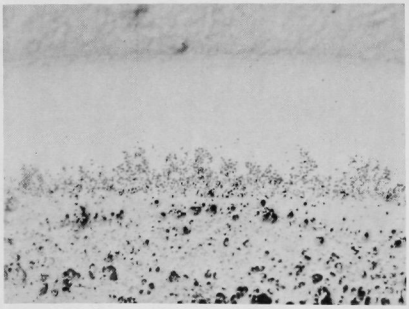

Fig. 43

Typical Reaction Zone between U-5 wt % Fs-2.5 wt % Zr Alloy and Niobium Cladding. (Specimen No. 15-2.) Mag. 200X. Neg. No. MSD-160613.

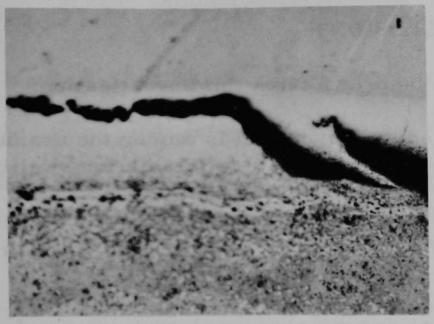

Fig. 44

Cracking in Reaction Zone between U-5 wt % Fs-2.5 wt % Zr Alloy and Niobium Cladding. (Specimen No. 15-2.) Mag. 200X. Neg. No. MSD-160609.

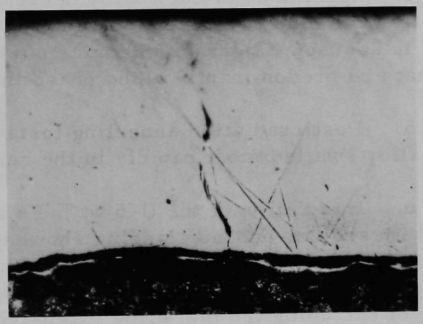

Fig. 45

Typical Reaction Zone between U-5 wt % Fs-2.5 wt % Zr Alloy and Vanadium Cladding. Crack is evident in the cladding. (Specimen No. 15-5.) Mag. 200X. Neg. No. MSD-160611.

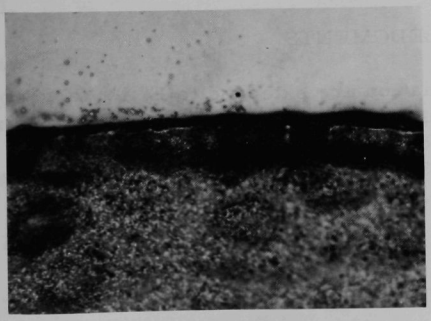

Fig. 46

Typical Reaction Zone between U-5 wt % Fs-2.5 wt % Zr Alloy and V-10 wt % Ti-3 wt % Nb Alloy Cladding. (Specimen No. 15-4.) Mag. 200X. Neg. No. MSD-160610.

VI. CONCLUSIONS

The following conclusions can be drawn from this investigation:

1. The U-5 wt % Fs alloy used as driver fuel is among the uranium-base alloys most capable of resisting high-temperature irradiation swelling.

2. None of the other alloys irradiated, including those with higher fissium and zirconium contents, showed a generally greater resistance to swelling under irradiation than the U-5 wt % Fs alloy.

3. No evidence of reversion to gamma phase was seen in any of alloys irradiated.

4. Specimens of each alloy decreased significantly in density when thermally cycled between the alpha and the alpha-plus-gamma temperature fields. In addition, slight anisotropic growth occurred in the alloy compositions that are predominantly alpha phase in the as-cast condition.

5. Postirradiation annealing tests of the alloys showed that the U-5 wt % alloy swelled most rapidly in the range 575-650°C.

6. Irradiation of the U-5 wt % Fs and U-5 wt % Fs-2.5 wt % Zr alloys with sodium-bonded cladding showed that (a) swelling of the alloys was effectively restrained by most of the 0.009-in.-thick cladding materials investigated; (b) the fuel developed local hydrostatic pressures that were capable of extruding the fuel alloy extensively out of small holes in the cladding; and (c) little axial movement of the fuel occurred within the cladding, even when the fuel was entirely unrestrained at its upper surface.

ACKNOWLEDGMENTS

Particular thanks and appreciation are extended to F. L. Yaggee, who fabricated and supplied all the fuel-alloy castings required for the experiments. In addition, we acknowledge the capable technical assistance of the reactor operating staffs of the MTR and CP-5 reactors as well as the hot-cell group of the ANL Materials Science Division.

REFERENCES

1. H. F. Jelinek, N. J. Carson, Jr., and A. B. Shuck, *Fabrication of EBR-II, Core-I Fuel Pins*, ANL-6274 (June 1962).

2. R. W. Bohl and M. V. Nevitt, *A Study of Uranium-Fissium Alloys Containing Technetium*, ANL-6495 (Oct 1962).

3. J. H. Monaweck and E. S. Sowa, *Summary Report on Irradiation of Prototype EBR-II Fuel Elements*, ANL-6010 (Sept 1960).

4. K. F. Smith, *Irradiation of Uranium-Fissium Alloys and Related Compositions*, ANL-5736 (Sept 1957).

5. J. A. Horak and J. H. Kittel, *Irradiation Behavior of U-Fs and U-Pu-Fs Fast Reactor Fuels*, Nucl. Met. *VI*, 35-38, Am. Inst. Min. and Met. Eng. (1959).

6. K. F. Smith and L. R. Kelman, *Irradiation of Cast Uranium-Plutonium Base Alloys*, ANL-5677 (May 1957).

7. J. A. Horak, J. H. Kittel, and R. J. Dunworth, *The Effects of Irradiation on Uranium-Plutonium-Fission Alloys*, ANL-6429 (July 1962).

8. W. N. Beck, J. H. Kittel, and R. J. Fousek, *Irradiations of U-20 Pu-10Fs Alloy Fuel Rods*, ANL-6750 (Feb 1965).

9. W. N. Beck, R. J. Fousek, and J. H. Kittel, *The Irradiation Behavior of High-burnup Uranium-Plutonium Alloy Prototype Fuel Elements*, ANL-7388 (May 1968).

10. S. T. Zegler and M. V. Nevitt, *Some Properties of Uranium-Fissium Alloys*, Nucl. Sci. Eng. *6*, 222-228 (1959).

11. M. V. Nevitt and S. T. Zegler, *Transformation Temperatures and Structures in Uranium-Fissium Alloys*, J. Nucl. Mat. *1*, 6-12 (1959).

12. S. T. Zegler and M. V. Nevitt, *Structures and Properties of Uranium-Fissium Alloys*, ANL-6116 (July 1961).

13. H. A. Saller, R. F. Dickerson, A. A. Bauer, and N. E. Daniel, *Properties of a Fissium-Type Alloy*, BMI-1123 (1956).

14. *Annual Report for 1958: Metallurgy Division*, ANL-5975, p. 57 (Mar 1959).

15. F. L. Yaggee, J. E. Ayer, and H. F. Jelinek, *Injection Casting of Uranium-Fissium Alloy Fuel Pins*, Nucl. Met. *IV*, 51-64, Am. Inst. Min. and Met. Eng. (1957).

16. J. E. Rein and B. F. Rider, *Burnup Determination of Nuclear Fuels*, TID-17385 (1963).

17. W. N. Beck, J. H. Kittel, and F. L. Brown, *Modification of CP-5 Fuel Assemblies for Fuel Capsule Irradiation Experiments*, ANL-6041 (Nov 1959).

18. W. N. Beck and R. J. Fousek, *Instrumented Temperature-controlled Capsules for Irradiations in the CP-5 Reactor*, ANL-6554 (Oct 1962).

19. W. N. Beck, *A Pinhole Camera Autoradiographic Technique for Encapsulated Irradiated Fuel Specimens*, ANL-6533 (Apr 1962).

20. J. H. Kittel, J. A. Horak, W. F. Murphy, and S. H. Paine, *Effects of Irradiation on Thorium and Thorium-Uranium Alloys*, ANL-5674 (Apr 1963).

21. B. R. Hayward and L. E. Wilkinson, *Radiation Behavior of Metallic Fuels for Sodium Graphite Reactors*, NAA-SR-3411 (1959).

22. J. E. Gates, G. E. Lamale, and R. F. Dickerson, *The Examination and Evaluation of Irradiated Thorium-11 w/o Uranium Specimens*, BMI-1334 (1959).

23. C. R. Hann and R. D. Leggett, *Examinations of EBR-II Fuel Pins at PNL*, BNWL-CC-1441 (1967).

24. M. L. Bleiberg, L. J. Jones, and B. Lustman, *Phase Changes in Pile-Irradiated Uranium-Base Alloys*, J. Appl. Phys. *21*, 1270-1283 (1956).

25. A. A. Shoudy, W. E. McHugh, and M. A. Sulliman, "The Effect of Irradiation Temperature and Fission Rate on the Radiation Stability of the Uranium-10 wt % Molybdenum Alloy," in *Radiation Damage in Reactor Materials*, 133-162, IAEA, Vienna (1963).

26. W. D. Wilkinson, *Uranium Metallurgy*, Volume II, 905, Interscience Publishers, New York and London (1962).

27. K. Matsumoto, unpublished work, Argonne National Laboratory.

28. N. R. Chellew and R. K. Steunenberg, *Fission Gas Release and Swelling During Heating of Irradiated EBR-II Type Fuel*, Nucl. Sci. Eng. *14*, 1-7 (1962).